The ^{129}Xe nuclear shielding surfaces for Xe interacting with linear molecules CO_2, N_2, and CO

Angel C. de Dios
Department of Chemistry, Georgetown University, 37th and O Streets N. W., Washington DC 20057-2222

Cynthia J. Jameson
Department of Chemistry M/C-111, University of Illinois at Chicago, 845 W. Taylor, Chicago, Illinois 60607

(Received 13 February 1997; accepted 12 June 1997)

We have calculated the intermolecular nuclear magnetic shielding surfaces for ^{129}Xe in the systems Xe–CO_2, Xe–N_2, and Xe–CO using a gauge-invariant *ab initio* method at the coupled Hartree–Fock level with gauge-including atomic orbitals (GIAO). Implementation of a large basis set (240 basis functions) on the Xe gives very small counterpoise corrections which indicates that the basis set superposition errors in the calculated shielding values are negligible. These are the first intermolecular shielding surfaces for Xe-molecule systems. The surfaces are highly anisotropic and can be described adequately by a sum of inverse even powers of the distance with explicit angle dependence in the coefficients expressed by Legendre polynomials $P_{2n}(\cos\theta)$, $n=0-3$, for Xe–CO_2 and Xe–N_2. The Xe–CO shielding surface is well described by a similar functional form, except that $P_n(\cos\theta)$, $n=0-4$ were used. When averaged over the anisotropic potential function these shielding surfaces provide the second virial coefficient of the nuclear magnetic resonance (NMR) chemical shift observed in gas mixtures. The energies from the self-consistent field (SCF) calculations were used to construct potential surfaces, using a damped dispersion form. These potential functions are compared with existing potentials in their predictions of the second virial coefficients of NMR shielding, the pressure virial coefficients, the density coefficient of the mean-square torque from infrared absorption, and the rotational constants and other average properties of the van der Waals complexes. Average properties of the van der Waals complexes were obtained by quantum diffusion Monte Carlo solutions of the vibrational motion using the various potentials and compared with experiment. © *1997 American Institute of Physics.* [S0021-9606(97)01835-7]

INTRODUCTION

The largest intermolecular chemical shifts in nuclear magnetic resonance spectroscopy have been observed for ^{129}Xe nucleus. The observed NMR chemical shifts are the differences in the magnetic response property, the nuclear magnetic shielding, in going from one electronic environment to another. The extremely high sensitivity of the ^{129}Xe NMR chemical shift to its environment has made the Xe atom a widely used probe in the characterization of microporous materials such as clathrates,[1,2] zeolites,[3–5] polymers,[6–8] graphite, coals, and other materials. In zeolites the ^{129}Xe chemical shift is known empirically to depend on zeolite pore and channel dimensions,[3–5] cation distribution,[9,10] dispersed metal atoms,[4,5,11,12] and domains of different composition or crystallinity.[13] An understanding of the sensitivity of the chemical shift to these parameters, crucial to the quantitative application of the empirical observations, still remains elusive.

While the Xe chemical shifts in heterogeneous porous solids are dramatically large, we begin our theoretical studies of Xe shielding by calculating the intermolecular shielding surfaces for Xe interacting with a single molecule rather than a liquid medium or a graphite sheet. The most quantitative comparisons can be made with the gas-phase density coefficients of the Xe chemical shifts that have been measured in the mixture of Xe with other gases.[14,15] In our earlier calculations of intermolecular shielding surfaces we have used the rare gas atoms He, Ne, and Ar to characterize the general shape of the intermolecular shielding surface for rare gas pairs. We have shown that the surface is nonmonotonic, is zero at large separations since the reference is the free atom, and becomes deshielding as the other atom or molecule is brought closer to the nucleus in question, goes to a minimum at a fairly short intermolecular separation and becomes more shielded in the approach toward the united atom limit.[16–18] It has been shown[16] that when the basis sets used (especially for the atom bearing the nucleus whose shielding is being calculated) are not saturated, the intermolecular shielding surface may exhibit a spurious positive shielding hump which disappears as soon as the basis set superposition errors are accounted for, for example, by adopting the Boys–Bernardi counterpoise corrections. Counterpoise corrections can be as large as a few ppm.[19] The ^{39}Ar shielding in Ar–Ne, the Ne shielding in Ne–Ne and Ne–He[17] and the He shielding in the He–He system[20] were found to have the same shape. The latter exhibited a minimum only at the correlated level of calculation, using multiconfiguration SCF wave functions in the individual gauge for localized orbitals

(MC-IGLO) whereas the correlation contributions to the ^{39}Ar shielding in the Ar–Ar system had been shown by second order localized orbital/local origin method (SOLO) calculations to be negligibly small. In all rare gas pairs the minimum in the shielding surface occurs at a distance much shorter than r_0, the separation at which the potential energy of interaction goes to zero.

The shapes of the intermolecular shielding surfaces for rare gas pairs are very similar and the nearly identical R dependence at separations around or larger than r_0, suggests that they may be conformal in the same sense that the law of corresponding states suggests that potential-energy surfaces are conformal.[16] It has been found that the rare gas intermolecular shielding functions do scale according to the factors $\alpha_A \cdot \langle a_0^3/r^3 \rangle_A \cdot \alpha_B \cdot U_A U_B/(U_A+U_B)$, for the shielding of A due to the presence of B, where α_A is the electric dipole polarizability of the rare gas atom in question and U_A is the first ionization potential of the atom. The characteristic $\langle a_0^3/r^3 \rangle$ of the free atom in its ground state is the factor for the intrinsic shielding sensitivity,[21,22] and, to the extent that the shielding response is effected by the mutual distortion of the electron charge distribution of each atom in the presence of the other atom, the magnitude of the response could be related to the usual quantities that appear in the London model for dispersion energy. The scaled ^{39}Ar in Ar–Ar shielding function produced curves that were nearly superposable in the range of distances of interest with the *ab initio* shielding functions of other rare gas pairs.[16] The ^{39}Ar shielding in Ar–Ar, scaled to the ^{129}Xe shielding in Xe–Ar, Xe–Kr, and Xe–Xe gives second virial coefficients of the ^{129}Xe shielding in rare gas mixtures which are in excellent agreement with experiment in sign, magnitude, and temperature dependence.[16] We have recently found that the *ab initio* shielding surface for Xe–Xe itself agrees quite well with the scaled Ar–Ar shielding surface over the range of distances that are important in the averaging over the Xe_2 potential surface.[23]

In this paper we report *ab initio* calculations of intermolecular shielding surfaces of Xe interacting with linear molecules CO_2, N_2, and CO. We examine the sensitivity of the ^{129}Xe shielding to the configuration of the supermolecule. In the process of doing the shielding calculations, we obtain $V^{\mathrm{SCF}}(R,\theta)$ with which we construct a potential-energy surface for the system. Finally, we average the intermolecular shielding over all configurations to obtain the temperature-dependent density coefficients of the ^{129}Xe NMR chemical shift and compare with the values that have been measured in gas-phase mixtures of Xe with these gases.[24,25]

METHODS

The ^{129}Xe intermolecular shielding surfaces for Xe–CO_2, Xe–N_2, and Xe–CO

In our previous work we have used the calculated shielding surface of the ^{39}Ar nucleus in systems in which Ar atom is interacting with another atom, ion, or molecule,[16–20] or even a fragment of a zeolite cage,[19] as a model for the shielding surface of the ^{129}Xe nucleus in a Xe atom in similar environments, converting the ^{39}Ar nuclear shielding to ^{129}Xe shielding by using scaling factors, as described above. In this paper, we report the ^{129}Xe intermolecular shielding surfaces for Xe in the systems Xe–CO_2, Xe–N_2, and Xe–CO carried out using the coupled Hartree–Fock method using gauge-including atomic orbitals (GIAO).[26] This is one of the four well established methods for shielding calculations using distributed origins. Other methods, localized orbital/local origin (LORG), individual gauge for localized orbitals (IGLO), and individual gauges for atoms in molecules (IGAIM) provide comparable results at the same basis set level.[27–31] Density functional methods using either IGLO or GIAO schemes have also been very successful.[32] The basis set on the Xe atom has to be large enough to accurately depict the response of the shielding tensor of the Xe nucleus to the linear molecule at various orientations and intermolecular separations. For this purpose we have used 240 basis functions on the Xe, uncontracted $29s\ 21p17d9f$. The core $(25s18p13d)$ was taken from Partridge and Faegri;[33] this was augmented by $3s$, $2p$, $4d$, and $9f$ orbitals with exponents taken from D. Bishop,[34] who had used these functions in shielding calculations of Xe atom in the presence of a uniform electric field. The basis set used for C and O are $11s7p3d$ contracted to $7s/6p/3d$. For N atom we used the $11s$, $7p$ Huzinaga basis[35] in the contraction $(5,6\times1;2,5\times1)$ augmented by two sets of d functions. In the calculation of the shielding surfaces of a rare gas atom in response to an aluminosilicate (zeolite) cage, the monomer (free Ar atom) shieldings to be used were calculated in the full supersystem (Ar plus zeolite fragment) basis. This is the so-called full counterpoise method. In these systems the basis set superposition errors BSSE in the ^{39}Ar shieldings is a function of position of the Ar with respect to the fragment and is of the order of a few ppm.[19] In contrast, the basis set used here for the Xe atom is large enough that the counterpoise correction to the ^{129}Xe shielding function was found to be negligible in every case, of the order of $+0.03$ ppm where the intermolecular shielding is -63.35 ppm (0.05%), and $+0.0006$ ppm where the intermolecular shielding is -5.0804 ppm (0.01%) for ^{129}Xe in Xe–CO, for example.

The *ab initio* values calculated at 70 (R,θ) points each for the ^{129}Xe intermolecular shielding in Xe–CO_2 and Xe–N_2 were fitted to the following functional form:

$$\{\sigma(R,\theta)-\sigma(\infty)\}=\sum_{p=6,\mathrm{even}}^{12} R^{-p} \sum_{\lambda=0,\mathrm{even}}^{6} a_{p\lambda} P_\lambda(\cos\,\theta), \tag{1}$$

where P_λ is a Legendre polynomial. The *ab initio* values at 130 (R,θ) points for ^{129}Xe intermolecular shielding in Xe–CO were fitted to the following function:

$$\{\sigma(R,\theta)-\sigma(\infty)\}=\sum_{p=6,\mathrm{even}}^{12} R^{-p} \sum_{\lambda=0}^{4} a_{p\lambda} P_\lambda(\cos\,\theta). \tag{2}$$

We use only even inverse powers of R even for this unsymmetrical case since the nucleus of interest resides in a molecule that has spherical symmetry.

An essential constraint that must be imposed on the fitting function is that the long-range behavior of the intermolecular shielding be correct. The *ab initio* points remain negative as r approaches large distances, up to 6 Å. The fitting was therefore constrained to keep the values of the function less than zero at 12 points: at 4, 5, 6, and 7 Å, at θ=0°, 45°, and 90°. If the fitting is allowed to be unconstrained at long range, the fitted function will have the wrong long-range behavior (a very low broad positive hump which integrates over the attractive part of the potential surface) and gives spurious positive contributions to $\sigma_1(\mathrm{Xe–CO_2})$.

We also considered fitting the shielding function to a sum of pairwise atom–atom radial only terms, such as

$$\{\sigma(R_1,R_2,R_3,\cdots)-\sigma(\infty)\} = \sum_i \left[a_{6i}R_i^{-6}+a_{8i}R_i^{-8}+a_{10i}R_i^{-10}+a_{12i}R_i^{-12}+\cdots\right], \tag{3}$$

where R_i is the distance between Xe and the ith atom in the linear molecule. This functional form has been used to describe the shielding function for a rare gas atom interacting with a zeolite fragment, in which i runs over as many as 52 atoms.[19] For these fitting functions, the behavior at large R_i is constrained so that each pairwise atom–atom function has the same behavior at very large separations as the total shielding itself, that is, $\{\sigma(R_1,R_2,R_3,\cdots)-\sigma(\infty)\}$ is monotonically negative at large distances.

The potential-energy surface (PES)

The individual contributions to the intermolecular potential can be calculated by various *ab initio* methods and then the calculated points are fitted to a parametrized functional form. It is useful to construct the potential-energy surface using the usual sum of contributions

$$V=V^{\mathrm{short}}+V^{\mathrm{elec}}+V^{\mathrm{ind}}+V^{\mathrm{disp}}. \tag{4}$$

It is common practice to associate V^{SCF}, the interaction energy evaluated from a SCF supermolecule calculation, with $V^{\mathrm{short}}+V^{\mathrm{elec}}+V^{\mathrm{ind}}$ so that

$$V=V^{\mathrm{SCF}}+V^{\mathrm{disp}}. \tag{5}$$

This neglects any dependence of the intramolecular correlation energy on the intermolecular coordinates, as well as various cross terms; it thus neglects the effects of intramolecular correlation on the repulsive potential and on the electrostatic and induction potentials. In the process of calculating the nuclear magnetic shielding of Xe at various interaction geometries with a linear molecule, we have obtained $V^{\mathrm{SCF}}(R,\theta)$ as a by-product. Thus, we can construct a potential-energy surface for the system at the same time as the construction of the ^{129}Xe intermolecular shielding surface.

We adopt the Tang and Toennies method of constructing the intermolecular potential, that is, by adding a damped dispersion contribution to the $V^{\mathrm{SCF}}(R,\theta)$. Just as important as the *ab initio* calculations at selected (R,θ) points in the configuration of the supermolecule, is the description of the surface in terms of a functional form. To describe V^{short}, we follow the suggestion by Buckingham, Fowler, and Hutson[36] and expand the reference distance and the exponent rather than $V^{\mathrm{short}}(R,\theta)$ itself in terms of angular functions. Thus, in the Xe–CO_2 case, the short range part of the potential itself is expanded as

$$V^{\mathrm{short}}(R,\theta)=A'\ \exp[-\beta(\theta)(R-R_{\mathrm{ref}}(\theta))], \tag{6}$$

where

$$R_{\mathrm{ref}}(\theta)=\sum_\lambda R_{\mathrm{ref},\lambda}P_\lambda(\cos\theta), \tag{7}$$

$$\beta(\theta)=\sum_\lambda \beta_\lambda P_\lambda(\cos\theta). \tag{8}$$

We thus fit $[V^{\mathrm{SCF}}(R,\theta)-V^{\mathrm{ind}}(R,\theta)]$ to this functional form to determine the parameters A', $R_{\mathrm{ref},\lambda}$ and β_λ, λ=0,2,4,6,8. $V^{\mathrm{SCF}}(R,\theta)$ is found from the Xe+CO_2 supermolecule *ab initio* calculations using GAUSSIAN 94[36(a)] (see below for counterpoise corrections), and $V^{\mathrm{ind}}(R,\theta)$ is taken from the theoretical expression appropriate for an atom and a linear molecule, given by Hettema *et al.*[37] with the electric moments of the linear molecule being taken from experiment or from *ab initio* calculations. $V^{\mathrm{ind}}(R,\theta)$ is added back to the function obtained by fitting Eq. (6).

The dispersion contribution at long range is of the form

$$V^{\mathrm{disp}}(R,\theta)=\sum_{n=6} -C_nR^{-n}, \tag{9}$$

$$C_n=\sum_\lambda C_n^{(\lambda)}P_\lambda(\cos\theta). \tag{10}$$

For Xe–CO_2 we have used λ=0,2,4,6,8 and n=6,8,10,12 with the dispersion coefficients $C_n^{(\lambda)}$ taken from T Pack.[38] At short range this behavior is modified using damping functions

$$V^{\mathrm{disp}}(R,\theta)=\sum_{n=6} -C_nR^{-n}D_n(R), \tag{11}$$

where $D_n(R)$ are the damping functions which are implicitly functions of orientation. We adopt the Tang–Toennies incomplete Γ function[39]

$$D_n(R)=1-\exp(-\beta R)\cdot\sum_{m=0}^{n}[(\beta R)^m/m!], \tag{12}$$

and β is set equal to the exponent used in the repulsive potential. The values of the coefficients used in this work and the parameters obtained from the fitting are given in Table I for the Xe–CO_2 system.

The problem of basis set superposition errors (BSSE) is of great importance not just in calculating interaction energies but also molecular electronic properties. The problem of BSSE, an explanation of its origin, and the methods of circumventing it have been reviewed.[40,41] BSSE in intermolecular shielding calculations is important since polarization functions and functions with diffuse exponents which are

TABLE I. Electric moments, dispersion coefficients, and fitting parameters for $Xe–CO_2$ molecular complex.[a]

λ	0	2	4	6	8	Ref.
$R_{\mathrm{ref},\lambda}$, Å	2.31022	0.679 603	−0.012 024 0	−0.003 797	0.009 035 6	this work
β_λ, Å^{-1}	3.11732	0.032 4677	0.158 266	−0.050 456 3	0.035 134 9	this work
A'	0.398 623					this work
$C_6^{(\lambda)}$, a.u.	282.	65.				38
$C_8^{(\lambda)}$, a.u.	6910.	5300.	1000.			38
α_1(Xe), a.u.	28.223					72
α_2(Xe), a.u.	223.29					72
$Q_2(CO_2)$, a.u.	−3.76					38
$Q_4(CO_2)$, a.u.	−0.06					38

[a]Units: a.u.$=ea_0^2$ for Q_2 (electric quadrupole moment), a.u.$=ea_0^4$ for Q_4 (electric hexadecapole moment), a.u.$=e^2a_0^2E_h^{-1}$ for α_1 (static dipole polarizability), a.u.$=e^2a_0^4E_h^{-1}$ for α_2 (static quadrupole polarizability), a.u.$=a_0^nE_h$ for $C_n^{(\lambda)}$ (dispersion coefficients).

employed in shielding calculations are readily used by all monomers in the complex and yield BSSE of the same order of magnitude as the interaction energy itself. Each subsystem (monomer) is calculated in the complete basis of the supersystem. In this work, the counterpoise correction,[42] the difference between an all-electron calculation on the $Xe–CO_2$ supermolecule and the sum of the Xe calculation in the presence of the CO_2 orbitals and the CO_2 calculation in the presence of the Xe orbitals, was not actually evaluated at every point in the $Xe–CO_2$ configuration space in which the SCF energies (and shielding functions) were calculated. Instead, the counterpoise correction was evaluated at a few selected geometries and the counterpoise correction to the SCF energy was fitted to the functional form $a\cdot[\exp(-br_1)+\exp(-br_2)]$ where r_1 and r_2 are the distances of the Xe from the two oxygen atoms of CO_2, and a and b are fitting parameters. It is the fitted function that is used to correct every point. For $Xe–CO_2$ the counterpoise corrections to the SCF energy were 36–60 microhartree in the range 3.4–4.4 Å, with only 0.5–1.0 μhartree coming from the inadequacies of the Xe basis set.

The $Xe–N_2$ potential-energy surface was constructed in a similar fashion, using the same functional forms as for $Xe–CO_2$. For this system, the dispersion coefficients and the terms in the induction energy have been calculated by Hettema *et al.*[37] We have used the values appropriate to the equilibrium geometry of N_2 which was assumed to be rigid in our *ab initio* calculations. The values of the coefficients used for $Xe–N_2$ and the parameters obtained from the fitting are given in Table II. For $Xe–N_2$ the counterpoise corrections to the SCF energy were larger, 90–160 μhartree in the range 3.4–4.4 Å, with only 0.4–1.2 μhartree coming from the inadequacies of the Xe basis set.

The Xe–CO potential-energy surface used the dispersion coefficients and the terms in the induction energy from Hettema *et al.*[37] After counterpoise corrections, $[V^{\mathrm{SCF}}(R,\theta)-V^{\mathrm{ind}}(R,\theta)]$ was fitted to Eq. (6)–(8) with λ=0,1,2,3,4 to describe the repulsive potential. For Xe–CO we have used

$$\begin{aligned}V^{\mathrm{ind}}(R,\theta)=&[C_6{}^{(0)\mathrm{ind}}+C_6{}^{(2)\mathrm{ind}}P_2(\cos\theta)]R^{-6}\\&+[C_7{}^{(1)\mathrm{ind}}P_1(\cos\theta)+C_7{}^{(3)\mathrm{ind}}P_3(\cos\theta)]R^{-7}\\&+[C_8{}^{(0)\mathrm{ind}}+C_8{}^{(2)\mathrm{ind}}P_2(\cos\theta)\\&+C_8{}^{(4)\mathrm{ind}}P_4(\cos\theta)]R^{-8},\end{aligned}\tag{13}$$

where the $C_n^{(\lambda)\mathrm{ind}}$ are taken from Hettema *et al.*[37] The $V^{\mathrm{disp}}(R,\theta)$ for Xe–CO is as in Eq. (10)–(12) with terms in λ=0,1,2,3,4 and n=6,7,8, with the dispersion parameters taken from Hettema *et al.* and the $\beta(\theta)$ in the damping function is set equal to the exponent found in the fitting of the repulsive potential. The values of the coefficients used for Xe–CO and the parameters obtained from the fitting are given in Table III. The counterpoise corrections to the SCF energy were 29–51 μhartree in the range 3.4–4.4 Å, with only 0.4–1.0 μhartree coming from the inadequacies of the Xe basis set.

TABLE II. Electric moments, dispersion coefficients, and fitting parameters for $Xe–N_2$ molecular complex.[a]

λ	0	2	4	6	8	Ref.
$R_{\mathrm{ref},\lambda}$, Å	1.427 49	0.306 507	0.025 400 5	−0.011 233 8	0.013 324 2	this work
β_λ, Å^{-1}	3.106 47	0.028 258 7	0.027 781 7	−0.009 226	0.01978	this work
A'	3.770 51					this work
$C_6^{(\lambda)}$, a.u.	139.5	12.39				37
$C_8^{(\lambda)}$, a.u.	5451.6	3029.7	−95.43			37
$C_{10}^{(\lambda)}$, a.u.	229 260.	176 685.	14 243.	−990.20		37
α_1(Xe), a.u.	28.223					72
α_2(Xe), a.u.	223.29					72
$Q_2(N_2)$, a.u.	−1.09					92
$Q_4(N_2)$, a.u.	−8.0					93

[a]Atomic units given in Table I.

TABLE III. Electric moments, dispersion coefficients, and fitting parameters for Xe–CO molecular complex.[a]

λ	0	1	2	3	4	Ref.
$R_{\mathrm{ref},\lambda}$, Å	1.379 43	−0.036 677 3	0.296 788	−0.059 262 8	0.088 768 9	this work
β_λ, Å^{-1}	3.085 47	0.217 892	−0.039 780 6	−0.025 562 5	0.146 271	this work
A'	4.153 40					this work
$C_6^{(\lambda)}$, a.u.	158.06		17.23			37
$C_7^{(\lambda)}$, a.u.		−460.64		15.29		37
$C_8^{(\lambda)}$, a.u.	6475.4		4300.		−193.6	37
α_1(Xe), a.u.	28.223					72
α_2(Xe), a.u.	223.29					72
Q_1(CO), a.u.	0.048					94
Q_2(CO), a.u.	−1.5					95
Q_3(CO), a.u.	3.879					37

[a]Units: a.u.$=ea_0$ for Q_1 (electric dipole moment), a.u.$=ea_0^2$ for Q_2 (electric quadrupole moment), a.u.$=ea_0^3$ for Q_3 (electric octopole moment), a.u.$=e^2a_0^2E_h^{-1}$ for α_1 (static dipole polarizability), a.u.$=e^2a_0^4E_h^{-1}$ for α_2 (static quadrupole polarizability), a.u.$=a_0^nE_h$ for $C_n^{(\lambda)}$ (dispersion coefficients).

The average properties of the Xe-linear molecule complex

Among the techniques that may be applied to the vibrational dynamics of a weakly bound complex is quantum diffusion Monte Carlo (QDMC). Anderson gave the first modern algorithm for simulating the Schrödinger equation as if it were a diffusion process.[43,44] With this we obtain the average rotational constants in the ground vibrational state. Consistent with the rigid geometry assumed for the linear molecule in the calculation of the intermolecular potential energy, we take the molecule to be rigid, as has been done by Buch and others.[45–47] The simulation consists of a number of copies of the system. Each copy is allowed to diffuse via a random walk process and to multiply or disappear with a probability determined by its potential energy. This process is repeated until the distribution of replicas approaches a fluctuating steady state from which the ground-state energy is evaluated. After equilibration, the simulation yields a collection of replicas of the system that have the statistical distribution which approaches the ground-state wave function of the system. Buch has implemented QDMC for two or more interacting molecules, each taken to be rigid, which we adopt here with no changes.[45] This treatment relies on the approximation that the high-frequency intramolecular vibrations are effectively decoupled from the lower-frequency intermolecular motions because these two types of motions occur at very different time scales. By eliminating the high-frequency motions the number of variables is decreased and larger time steps may be taken. Our simulations consisted of an equilibration phase lasting 600 time steps before the data collection phase. The number of replicas in all calculations was 5000. In each QDMC run the first 600 steps were carried out with time step of 150–200 a.u. after which the time step was decreased to 30 a.u. It is important that the first steps on the simulation are done with long enough time steps to probe a large region of the PES. Rotational constants and all other properties averaged over the zero-point motion were calculated by the method of descendant weighting which provides the means of obtaining expectation values from the distribution generated by QDMC.[48,49] The descendant weighting procedure used to obtain the averages was adopted from Ref. 50. The averaging was performed for 12 generations of replicas simultaneously at a delay of 100 steps between the consecutive generations. The descendants were collected after a delay of 500 steps for 1000 steps. The ground-state energy is obtained from the requirement of stability of the asymptotic average number of replicas. For a given potential-energy surface of CO_2–Xe, from the QDMC simulations we obtain the average rotational constants A, B, C for the ground vibrational state, the ground-state zero-point energy (and thus the dissociation energy D_0). These average quantities will be compared with the experimental values.

In the case of Xe–CO_2, the force constants for the van der Waals bend and stretch have been determined from the spectra.[51] These can be compared with the analytic second derivatives of the intermolecular potential. Furthermore, the stretching and bending frequencies of the van der Waals complex can be estimated using the GF matrix method of Wilson[52] considering both the inter- and the intramolecular interactions (force fields) simultaneously. The original molecular geometry of the linear molecule is employed in the calculation, any molecular distortion due to the intermolecular interaction within the complex is ignored. This is the total force field-unrelaxed molecule approach of Li and Bernstein.[53] The GF matrix diagonalization is an effective method for determination of the harmonic normal modes of van der Waals complexes. The intramolecular force field of the linear molecule was based on the spectroscopy of the isolated linear molecule. The intermolecular force field is directly calculated from derivatives of the intermolecular potential energy surface.

Second virial coefficients

There are three virial coefficients that we can use for testing the calculations on Xe–CO_2. The pressure second virial coefficient, the second virial coefficient of the nuclear shielding, and the density coefficient of the mean-square torque from infrared absorption, $\langle C^2\rangle/\rho$. All three involve an integration of an angle-dependent function over the aniso-

tropic potential surface. The pressure second virial coefficient can be calculated in the conventional way from the potential-energy surface,

$$B_{12}(T)=B_{12}^{\text{class}}(T)$$
$$=2\pi N_0\int\int\{1-\exp[-V(R,\theta)/k_BT]\}R^2$$
$$\times\sin\theta\,d\theta\,dR. \tag{14}$$

The first translational and rotational quantum corrections[54,55] are small and were not included. The mixed second virial coefficient of the nuclear shielding, $\sigma_1(\text{Xe–CO}_2)$, is the contribution of Xe–CO_2 interactions to the shielding $\sigma(T,\rho_{\text{Xe}},\rho_{\text{CO}_2})$ of Xe in the gas phase mixture of Xe and CO_2.

$$\sigma(T,\rho_{\text{Xe}},\rho_{\text{CO}_2})=\sigma(\text{free Xe atom})+\sigma_1(\text{Xe–Xe})\rho_{\text{Xe}}$$
$$+\sigma_1(\text{Xe–CO}_2)\rho_{\text{CO}_2}+\cdots. \tag{15}$$

This is calculated from the intermolecular shielding surface by

$$\sigma_1(\text{Xe–CO}_2)=2\pi N_0\int\int\{\sigma(R,\theta)-\sigma(\infty)\}$$
$$\times\exp[-V(R,\theta)/k_BT]R^2\sin\theta\,d\theta\,dR. \tag{16}$$

The mean-square torque $\langle C^2\rangle$ is related to the second and fourth spectral moments of the absorption profile of an IR absorption band and the rotational constant B,[56]

$$\langle C^2\rangle=[M(4)-2M^2(2)]/4B^2. \tag{17}$$

In the binary collision limit, Armstrong *et al.*[57] have written $\langle C^2\rangle$ in terms of an integral over the angular derivative of the interaction potential, $V(R,\theta)$

$$\langle C^2\rangle/\rho_{\text{Xe}}=2\pi N_0\int\int(\partial V(R,\theta)/\partial\theta)^2$$
$$\times\exp[-V(R,\theta)/k_BT]R^2\sin\theta\,d\theta\,dR, \tag{18}$$

where ρ_{Xe} is the number density of the perturbing gas in the CO_2–Xe system in which the CO_2 IR bands are observed. These three density coefficients are sensitive to the potential surface in different ways and therefore provide complementary experimental information about the potential-energy surface.

RESULTS

The Xe–CO_2 system

The intermolecular shielding values and the fitted function of the form given in Eq. (1) for ^{129}Xe in Xe–CO_2 are shown in Fig. 1. The trace for $R(\text{Xe-c.m.})=3.0$ Å has a spurious behavior at angles $\theta<40°$ and $\theta>140°$ where no *ab initio* calculations were carried out. The function of the form given in Eq. (1) gives a reasonably good description of the *ab initio* values of intermolecular shielding. The root mean-square deviation of this fit was 1.37 ppm. We have also attempted to describe the intermolecular shielding surface for Xe in this system by using a sum of pairwise additive atom–atom radial functions, (a site–site type of shielding function) as in Eq. (3). The fit is shown in Fig. 2, which may be compared to Fig. 1. Even at large distances, the fit to a function with an explicit angle dependence is superior to the sum

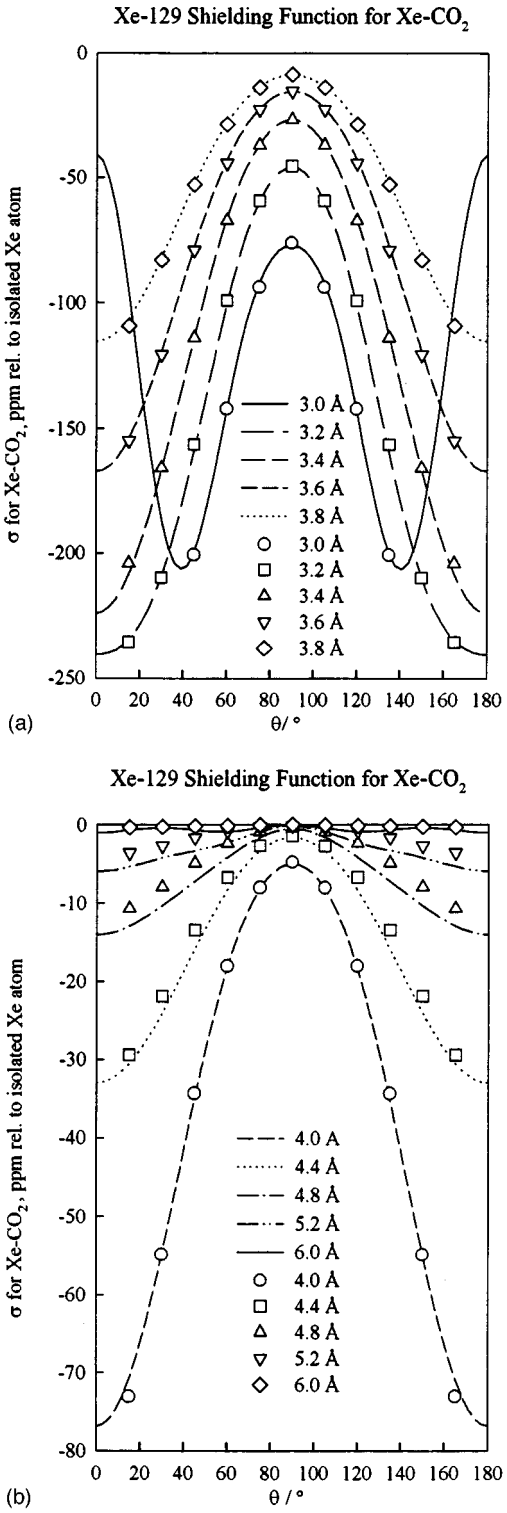

FIG. 1. The ^{129}Xe intermolecular shielding surface from *ab initio* calculations in Xe–CO_2 and the fitted function of the form given in Eq. (1).

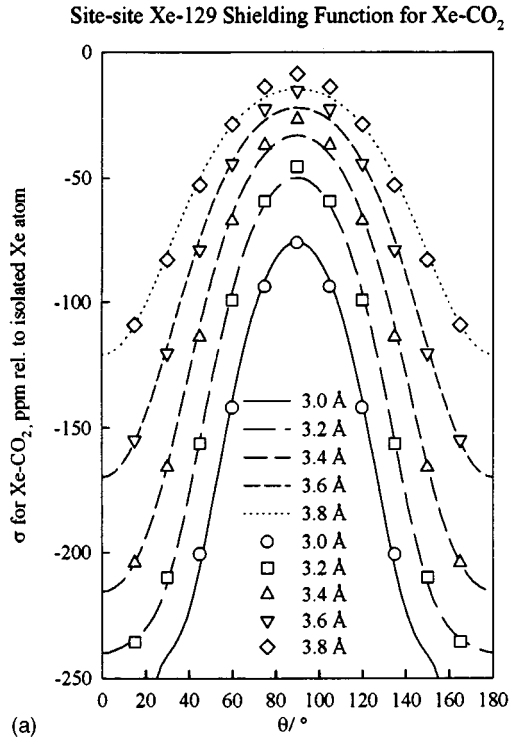

FIG. 2. The ^{129}Xe nuclear shielding for Xe–CO_2 described by a sum of pairwise atom–atom contributions [Eq. (3)].

of pairwise atom–atom terms. We find that the pairwise sum is inadequate to describe fully the intermolecular shielding surface at short distances where the anisotropy is very pronounced, as in these Xe-linear molecule cases. This is analogous to the relatively poorer performance of atom–atom pairwise potentials in representing the calculated potential energy of interaction between an atom and a linear molecule or between two linear molecules. We find that the site–site fit of the Xe–CO_2 shielding surface (standard deviation $=2.58$ ppm) gives a somewhat better description of the shielding values at small angles but does a much poorer job around $\theta=90°$, uniformly overestimating the magnitude of the deshielding effect at this geometry. Since the minimum energy structure of the Xe–CO_2 system is at $\theta=90°$, this is a serious defect of the site–site functional form. We therefore have used the fit to Eq. (1) in the rest of this work.

The induction and counterpoise corrections to the *ab initio* values of $V^{\mathrm{SCF}}(R,\theta)$ were carried out and $V^{\mathrm{short}}=[V^{\mathrm{SCF}}(R,\theta)-V^{\mathrm{ind}}(R,\theta)]$ was fitted to Eqs. (6)–(8). The potential function for the Xe–CO_2 system constructed in this work, using damped dispersion terms according to Eqs. (10)–(12), with dispersion coefficients from Pack[38] is shown in Fig. 3 and its characteristics are summarized in Table IV. When Fig. 3 is compared to the published potential of Buck *et al.*[58] shown in Fig. 4, the most obvious difference is the smaller curvature at the bottom of the Buck potential compared to the one constructed here. Since both ours and the Buck potential included the same dispersion coefficients from Pack,[38] the smaller curvature at the bottom of the well for the Buck potential is associated with the Buck functional form including only up to $P_2(\cos\theta)$ in the expansion in the repulsive part. We also found a smaller curvature in our fitted function when we truncated our angular dependence after the P_2 term. Our *ab initio* values for V^{short} are consistent with a narrower well region, however. Some of the parameters in the Buck potential were obtained from similarity considerations from the calculated or measured shape of the other rare gas–CO_2 complexes. The parameters R_0 and R_2 in the exponent of the repulsive term were determined from the condition that the minimum configuration occurs in the perpendicular approach with a large difference of the minimum distances $R_m(90°)=3.83$ Å and $R_m(0°)=5.29$ Å at well depths 33.6 and 8.29 meV, respectively.[58] The value of one of these parameters (R_2) is critical to whether a pronounced multiple collision rainbow will be observed, and indeed the crossed molecular beam experiments formed the basis for the choice of this parameter in the potential constructed by Buck *et al.* The characteristics of this potential are shown in Table V.

The Billing potential[59] also uses the Pack dispersion coefficients[38] in the long-range interaction.

$$V=V_{\mathrm{SR}}(1-h)+hV_{\mathrm{LR}}.$$

The short-range interaction is represented [in the same (R,θ) coordinates that we have used] by a dumbbell potential of the form

$$V_{\mathrm{SR}}^{0}=C[\exp(-\alpha R_1)+\exp(-\alpha R_2)]+B\exp(-\beta R),$$

where

$$R_1=R+d\cos\theta+0.5d^2\sin^2\theta/R,$$

$$R_2=R-d\cos\theta+0.5d^2\sin^2\theta/R,$$

$$\alpha=\alpha_0+\alpha_1R+\alpha_2R^2.$$

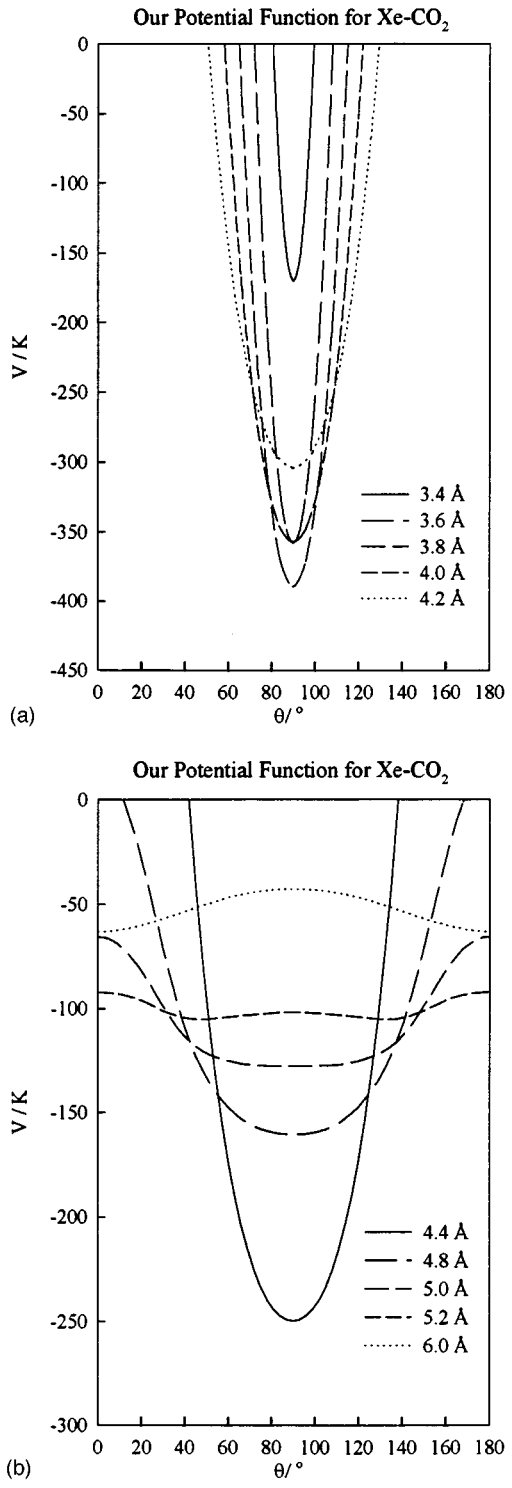

FIG. 3. The potential-energy surface for Xe–CO_2, this work.

The parameters B, d, α_0, α_1, α_2, were obtained by fitting to the electron gas calculations of Dreyfus[60] and C is a correction factor equal to 0.6553. The switching function is

$$h(R)=1, \quad R>\overline{d},$$

$$h(R)=\exp[-a(\overline{d}/R-1)^2], \quad R\leqslant\overline{d},$$

where $a=a_0+a_2P_2(\cos\theta)$.

TABLE IV. Characteristics of the Xe–CO_2, Xe–N_2, and Xe–CO potential-energy surfaces developed in this work.[a]

	Xe–CO_2	Xe–N_2	Xe–CO[b,c]
ϵ/k_B (90°)	390.09	131.25	141.05
R_m (90°)	3.768	4.218	4.186
σ (90°)	3.314	3.752	3.718
ϵ/k_B (0°)	95.19	97.26	133.32
R_m (0°)	5.319	4.763	4.449
σ (0°)	4.827	4.294	4.000
ϵ/k_B (180°)			58.60
R_m (180°)			5.308
σ (180°)			4.790

[a]Energies are in Kelvin and distances are in Å.
[b]θ=0° corresponds to CO···Xe, θ=180° to Xe···CO arrangement.
[c]Global minimum is at R=4.183Å, θ=88.7°, −141.12 K.

To find the parameters a_0, a_2, $\overline{d}$ in the switching function, Billing used the magnitude and positions of the minima in the parallel and perpendicular geometry from Buck *et al.*[58] The characteristics of this potential are given in Table V.

The function constructed by Iida, Ohshima, and Endo[51] is of the form

$$V(R,\theta)=C_{12}(\theta)R^{-12}-C_6(\theta)R^{-6}$$
$$-(9/2)Q^2_{CO_2}\alpha_{Xe}[P_2(\cos\theta)]R^{-8},$$

where only terms up to $P_2(\cos\theta)$ were used in $C_{2n}(\theta)=C^{(0)}_{2n}+C^{(2)}_{2n}P_2(\cos\theta)+\cdots$. $C^{(0)}_6$ was taken from T Pack[61] and $C^{(2)}_6=C^{(0)}_6(\alpha_\parallel-\alpha_\perp)/(\alpha_\parallel+2\alpha_\perp)$ was used. $C_{12}(90°)$ is obtained from the stretching force constant when the $C_6(90°)$ from above is used, and $C^{(2)}_{12}$ is obtained from the bending force constant when the $C^{(2)}_6$ from above is used. The van der Waals force constants were taken from their experimental data.[51] The characteristics of this potential are given in Table V.

The various potentials for Xe–CO_2 predicted second pressure virial coefficients which are compared with experimental values of $B_{12}(T)$[62] in Fig. 5. The Buck potential gives excellent agreement with the pressure second virial coefficient, reproducing 97% and 95% of the experimental values at 223 and 273 K,[62] whereas our potential function for Xe–CO_2 only finds 81% of the experimental values. The Billing function predicts 72% and 66% of the experimental values at 223 and 273 K. The Iida function, which was fitted to spectroscopic data for the van der Waals complex, gives even worse results. The Iida function gives 63% of the experimental pressure second virial coefficients.

The mean-square torque was calculated using Eq. (18) and the results are shown in Table V. Although there is no experimental value for the mean-square torque for Xe–CO_2 system itself, there are a series of rare gas measurements with CO_2[63] and with NNO.[64] For the series Ne, Ar, Kr, Xe, $\langle C^2\rangle/\rho$ for NNO at 300 K is, respectively, 390, 760, 1090, 1730 cm^{-2} $amagat^{-1}$.[64] On the other hand, for the series Ne, Ar, Kr, $\langle C^2\rangle/\rho$ for CO_2 at 300 K is respectively 300, 690, 925 cm^{-2} $amagat^{-1}$.[63] Therefore, we would expect that for CO_2–Xe $\langle C^2\rangle/\rho$ should be about 1500 cm^{-2} $amagat^{-1}$. On the other hand, Bulanin *et al.*[65] have reported mean-square

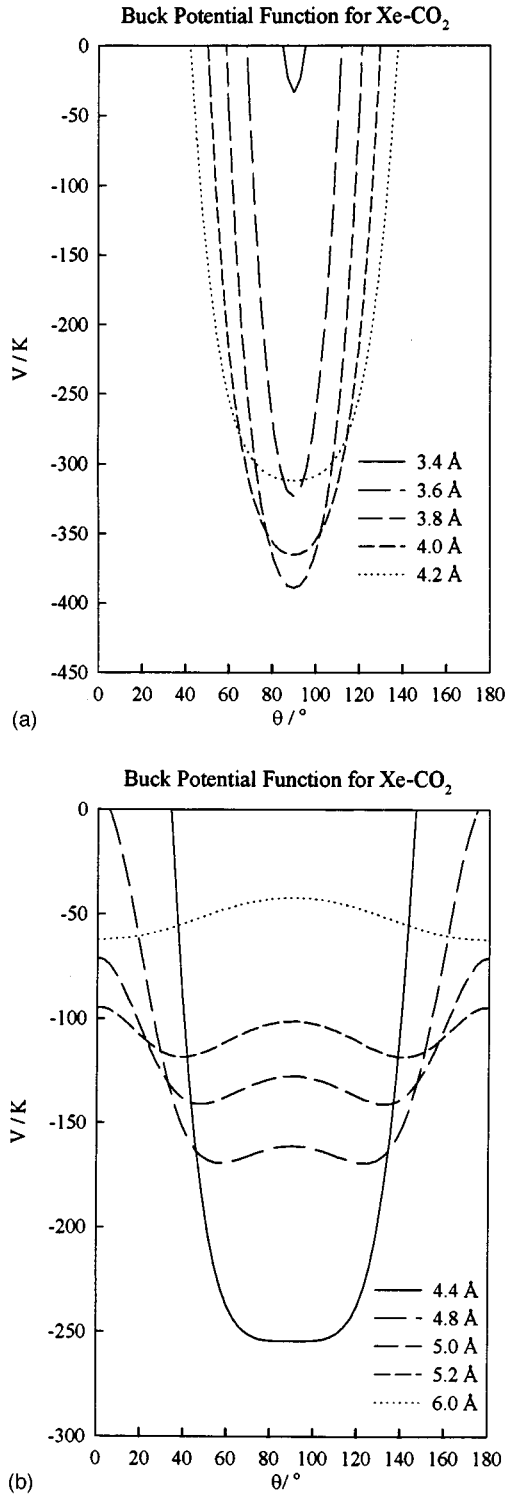

FIG. 4. The Buck potential surface for Xe–CO_2.

torques for CO_2–Ar and CO_2–Xe, respectively, 2000 ± 1000 and 5000 ± 2000 cm^{-2} amagat^{-1}, larger than the ones from Berreby and Dayan, but with much larger uncertainties as well. We believe that the Berreby and Dayan data are more reliable. We see that $\langle C^2\rangle/\rho$ predicted by the various potentials are in the range 2760–3410 cm^{-2} amagat^{-1}.

Using our calculated intermolecular shielding function for Xe–CO_2 to calculate the second virial coefficient of the ^{129}Xe intermolecular nuclear shielding as in Eq. (16), we find the predictions of the three Xe–CO_2 potential functions for the temperature dependence of this observable. In Fig. 6 the experimental values of the density coefficients of ^{129}Xe chemical shifts that we had previously measured in mixtures of Xe and CO_2,[24] are best predicted by the Buck potential, recovering 83% of the experimental σ_1(Xe–CO_2) value at 300 K. Our potential function and the Billing potential do not do as well, recovering only 68% of this value. These three potential functions give reasonably good accounting of the temperature dependence. However, the Iida potential predicts the wrong behavior of σ_1(Xe–CO_2) with temperature although it has 96% of the value at 300 K.

The average rotational constants for the Xe–CO_2 van der Waals complex are obtained from the pulsed nozzle Fourier transform microwave spectroscopy of the complex,[51] or from IR spectroscopy in the region of the ν_3 of CO_2.[66] In Table V the QDMC results are compared with the experimental values. The Buck potential has the proper shape at the global minimum to reproduce the van der Waals bend and stretch force constants reported by Iida *et al.*[51] from the pulsed Fourier transform microwave spectroscopy of this complex. On the other hand, our potential has larger second derivatives at the minimum and this translates to a greater bend force constant than the experimental one reported by Iida *et al.* Using our potential, we find 106% and 146% of the reported stretching and bending frequencies, whereas using Buck's potential, we get 111% and 89%, respectively. We find that the Billing potential gives the best agreement with the rotational constants and the best average distance. Our potential gives the next best agreement with rotational constants, followed by the Buck potential. The Iida potential gives the worst rotational constants, although the experimental force constants had been used to construct this potential.

Overall, the Buck potential appears to be the best practical potential insofar as the three different second virial coefficients are concerned, in addition to giving a very good agreement with spectroscopic data of the van der Waals complex. This potential was also found to provide satisfactory agreement with the experimental results in crossed molecular beam experiments; in particular it accounted for the large intensity peak in the molecular beam differential energy loss spectra which has been assigned to a multiple collision rotational rainbow.[67]

The Xe–N_2 system

The intermolecular ^{129}Xe shielding values calculated for the Xe–N_2 system were fitted to Eq. (1). The *ab initio* values and the fitted function are shown in Fig. 7. This angle-dependent description gives a good description of the calculated values. The root mean-square deviation of this fit was 0.74 ppm. Fitting to Eq. (3) using a sum of pairwise Xe–N shielding function leads to a poorer fit than the explicitly angle-dependent Eq. (1). The anisotropy of the shielding surface is not as pronounced as in Xe–CO_2.

The characteristics of the potential function for the

TABLE V. The PES for Xe–CO_2 and predictions of constants derived from spectroscopy.

Observable	Expt.	Buck	Billing	Iida	*Ab initio*
k_s, mdyne/Å	0.021 460(2)[e]	0.026 786[a]	0.028 239[a]	0.0191(18)[e]	0.024249[a]
k_b, mdyne·Å	0.012 556(10)[e]	0.010 00[a]	0.031 916[a]	0.0125[e]	0.026675[a]
ω_s, cm^{-1}	33.2[e]	37.0[b]	38.0[b]	31.3[b]	35.2[b]
ω_b, cm^{-1}	32.8[e]	29.3[b]	52.4[b]	32.7[b]	47.8[b]
$\langle C^2\rangle/\rho$ cm^{-2}/amagat	1500 (est.)	2761[d]	3411[d]	904[d]	3194[d]
	3.8154[f]				
$\langle R_m\rangle$, Å	3.818[e]	3.8784(24)[c]	3.8101(11)[c]	3.8959(12)[c]	3.8407(14)[c]
A, MHz	11 880.40(65)[e]	11 906.7(25)[c]	11 827.4(22)[c]	11 899.1(26)[c]	11 837.2(13)[c]
B, MHz	1057.7867(31)[e]	1021.1(12)[c]	1058.6(6)[c]	1012.65(68)[c]	1041.86(75)[c]
C, MHz	966.8030(30)[e]	940.1(10)[c]	971.3(5)[c]	932.83(57)[c]	957.24(64)[c]
D_0, cm^{-1}		238.57(76)[c]	234.05(30)[c]	163.87(17)[c]	231.38(9)[c]
ϵ/k_B (90°), K	390.[g]	389.74	398.86	279.33	390.09
R_m (90°), Å	3.83[g]	3.818	3.740	3.817	3.768
σ (90°), Å		3.386	3.315	3.402	3.314
ϵ/k_B (0°), K	96.2[g]	96.20	104.86	127.56	95.19
R_m (0°), Å	5.29[g]	5.294	5.184	4.638	5.319
σ (0°), Å		4.811	4.735	4.134	4.827

[a]From analytic derivatives of the potential function at the global minimum.
[b]Harmonic van der Waals stretching and bending frequencies from diagonalization of the GF matrix using k_s and k_b values in this table.
[c]From quantum diffusion Monte Carlo solution of the van der Waals vibrational motion. These are averages over the ground-state vibrational wave functions.
[d]From integration according to Eq. (18).
[e]Reference 51.
[f]Reference 66.
[g]Reference 58.

Xe–N_2 system constructed in this work, using damped dispersion terms according to Eq. (10)–(12), and dispersion coefficients from Hettema *et al.*[37] are summarized in Table IV. We may compare the potential function for Xe–N_2 constructed in this work with the potential surface published by Kistemaker and de Vries[68] and with four potential functions constructed by ter Horst.[69] These potentials have various forms: Kistemaker and de Vries proposed a set of N_2-rare gas surfaces which are sums of site-to-site Morse functions, with parameters determined by using combining rules.

$$V(r_1,r_2)=A\cdot\exp[-2\alpha(r_1-r_m)]-2B\cdot\exp[(-\alpha(r_1-r_m)] + A\cdot\exp[-2\alpha(r_2-r_m)]-2B\cdot\exp[(-\alpha(r_2-r_m)], \tag{19}$$

where r_1 and r_2 are the Xe–N distances; A, B, α, and r_m are parameters found by fitting the spherical part of the above potential to the spherical Morse potential whose parameters were obtained by combining rules from N_2–N_2 and the rare gas potentials.

Four potentials constructed by ter Horst,[69] designated BTT, TNTA, TNTB, and MNT are based on the Tang and Toennies model[70] in which

$$V(R,\theta)=V_0(R)+V_2(R)P_2(\cos\theta)+V_4(R)P_4(\cos\theta). \tag{20}$$

The radial contributions are determined from linear combinations of cuts of the surface at 0° and 90°, and only terms up to $P_2(\cos\theta)$ were included

$$V_0(R)=\{V(R,0°)+2V(R,90°)\}/3, \tag{21a}$$

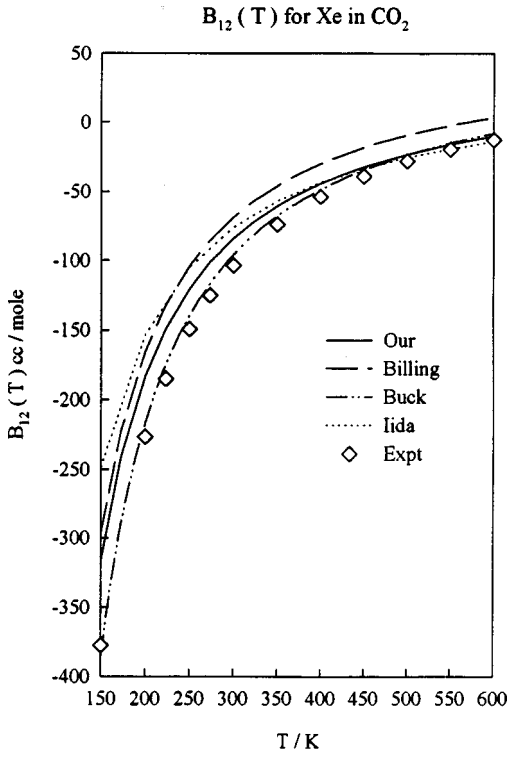

FIG. 5. The pressure second virial coefficient predicted by various potential surfaces are compared against the experimental data. The experimental points at 223 and 273 K are from the measurements of Brewer and the other ''experimental'' points are based on Brewer's universal correlating equation for second virial coefficients using a corresponding states approach. (Ref. 62).

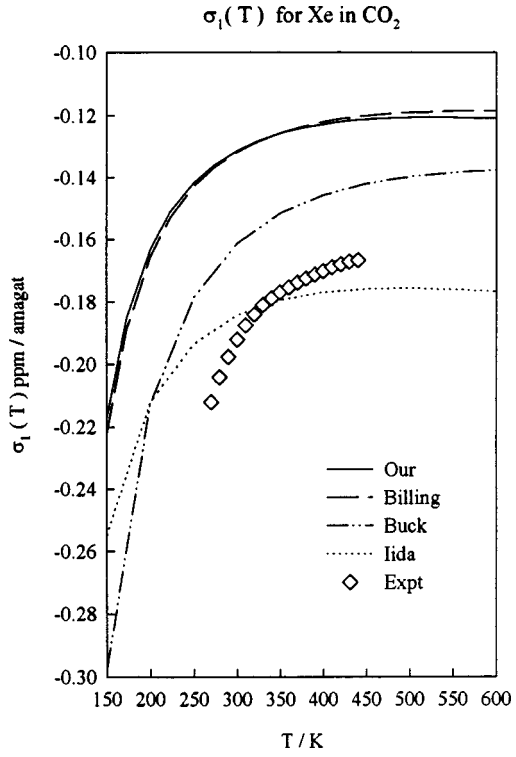

FIG. 6. The predicted second virial coefficients of ^{129}Xe nuclear shielding for Xe–CO_2 calculated by averaging the *ab initio* Xe–CO_2 shielding surface using various potential functions are compared with the experimental data obtained in the gas phase (Ref. 24).

$$V_2(R)=2\{V(R,0°)-V(R,90°)\}/3. \tag{21b}$$

Each cut $V(R,\theta_0)$ is written as a combination of a Born–Mayer repulsive term and a damped dispersion term

$$V(R,\theta_0)=A(\theta_0)\exp[-\beta(\theta_0)R] - \sum_{n\geqslant 3}^{n\ \max}\left\{1-\exp[-\beta(\theta_0)R]\cdot\sum_{k=0}^{2n}[\beta(\theta_0)R]^k/k!\right\}\cdot C_{2n}(\theta_0)R^{-2n}, \tag{22}$$

where n max=8 and,

$$C_{2n}(\theta_0)=C_{2n}^{(0)}+C_{2n}^{(2)}\cdot P_2(\cos\ \theta)+\cdots+C_{2n}^{(2n-4)}\cdot P_{2n-4}(\cos\ \theta). \tag{23}$$

The Born–Mayer parameters for N_2–Xe taken from Nyeland and Toennies[71] were used in the BTT, TNTA, TNTB, and MNT potentials. The differences between these PES lie in the dispersion terms. TNTA and TNTB use the dispersion coefficients from Thakkar *et al.* The TNTB function used just the same set of dispersion coefficients we have used, except that ter Horst used $C_6^{(0)}$ and $C_6^{(2)}$ scaled by the constrained dipole oscillator strength distribution (DOSD) values, as recommended by Hettema *et al.*[37] The TNTA surface used the earlier Thakkar values of dispersion coefficients.[72] The MNT surface used estimates of dispersion coefficients from McCourt,[73] which are based on the systematic relations between N_2–rare-gas dispersion coefficients with increasing rare gas polarizability [these include only up to $P_2(\cos\theta)$ terms]. The BTT surface uses the dispersion coefficients from Bowers and Tang[70] with C_{12} terms added on. The values of $C_{12}^{(0)}$ and $C_{12}^{(2)}$ were obtained by using the combining rule,[74]

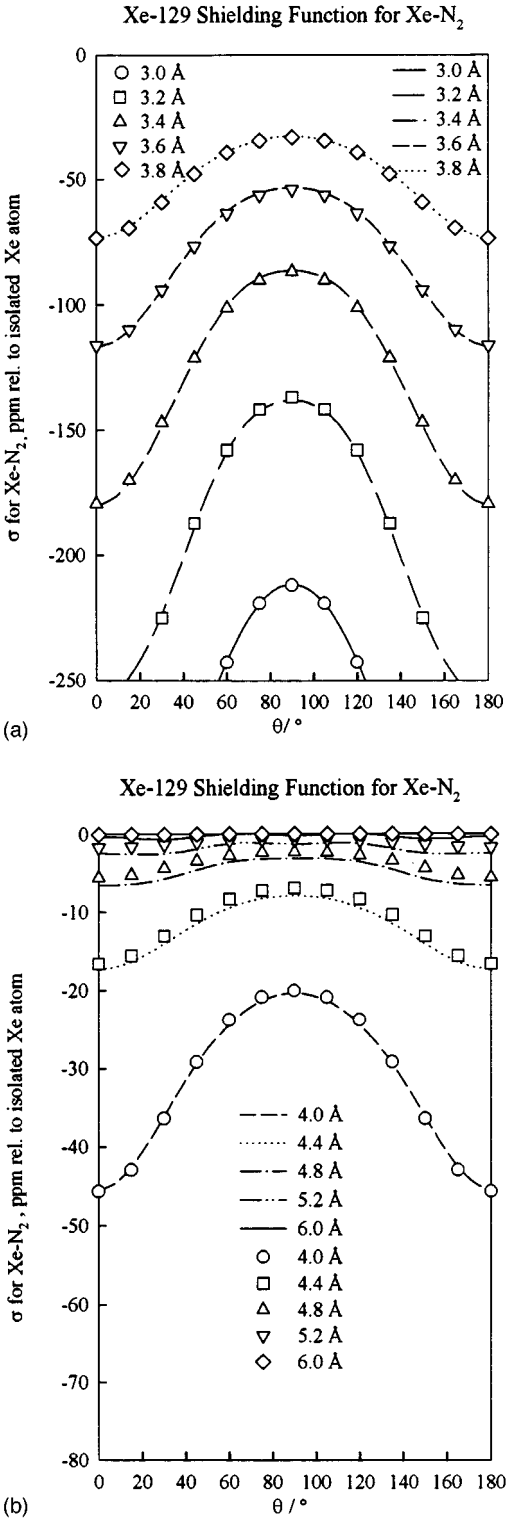

FIG. 7. The ^{129}Xe intermolecular shielding surface from *ab initio* calculations in Xe–N_2 and the fitted function of the form given in Eq. (1).

TABLE VI. The PES for Xe–N_2 and predictions of constants derived from spectroscopy.

Observable	kdV	BTT	TNTA	TNTB	MNT	*Ab initio*
k_s, mdyne/Å	0.012 191[a]	0.017 526[a]	0.013 838[a]	0.013 179[a]	0.018 014[a]	0.007 698[a]
k_b, mdyne.Å	0.001 725[a]	0.006 248[a]	0.005 199[a]	0.005 104[a]	0.009 369[a]	0.000 629[a]
$\langle R_m \rangle$, Å	4.0581(12)[b]	4.0279(16)[b]	4.1442(7)[b]	4.1584(13)[b]	4.0065(27)[b]	4.3897(11)[b]
A, MHz	68 862(495)[b]	65 293(282)[b]	66 486(250)[b]	66902(144)[b]	63225(51)[b]	$90.2(36)\times10^{3}$[b]
B, MHz	1333.72(90)[b]	1354.1(11)[b]	1279.44(39)[b]	1271.17(77)[b]	1368.8(17)[b]	1140.27(60)[b]
C, MHz	1306.91(86)[b]	1325.6(10)[b]	1254.29(39)[b]	1246.38(74)[b]	1339.4(16)[b]	1121.83(58)[b]
D_0, cm^{-1}	134.66(8)[b]	134.47(14)[b]	108.58(13)[b]	102.80(33)[b]	131.30(21)[b]	74.28(7)[b]
ϵ/k_B (90°), K	231.3	247.1	204.1	194.9	251.1	131.2
R_m (90°), Å	3.945	3.891	3.984	4.000	3.873	4.218
σ (90°), Å	3.444	3.465	3.551	3.565	3.452	3.752
ϵ/k_B (0°), K	163.4	178.5	142.1	132.0	129.5	97.3
R_m (0°), Å	4.422	4.451	4.563	4.586	4.582	4.763
σ (0°), Å	3.927	4.016	4.117	4.139	4.138	4.294

[a]From analytic derivatives of the potential function at the global minimum.
[b]From quantum diffusion Monte Carlo solution of the van der Waals vibrational motion. These are averages over the ground-state vibrational wave functions.

$$C_{2n}(\theta_0) = C_{2n-6}(\theta_0)[C_{2n-2}(\theta_0)/C_{2n-4}(\theta_0)]^3. \qquad (24)$$

The TNTA and TNTB potential functions go up to C_{10} terms. The parameters used in these four potential surfaces are given in Ref. 69. The characteristics of these surfaces are summarized in Table VI. It should be noted that our potential is much more shallow in the global minimum than these others. In fact the potential constructed here for Xe–N_2 is *too shallow* (131 K) compared to Ar–N_2 (153 K)[75] and Kr–N_2 (194–251 K).[76,77]

The $B_{12}(T)$ predicted by the various potential surfaces for Xe–N_2 are shown in Fig. 8. Our potential function for Xe–N_2 only finds 53% and 42% of the experimental values of the pressure second virial coefficients at 223 and 273 K.[62] The other potential functions do much better. The TNTA potential surface gives the best agreement with experiment, the MNT surface giving also reasonably good results. The BTT surface gives magnitudes much too large while our surfaces gives magnitudes much too small.

We see in Fig. 9 that only our potential gives a reasonable agreement with the experimental temperature dependence of the density coefficients of ^{129}Xe chemical shifts that we had previously measured in mixtures of Xe and N_2,[25] although ter Horst's various potentials give about the right magnitude at room temperature. Our potential has the right behavior with temperature, recovering 72% of the experimental value at 300 K. When this second virial coefficient of Xe shielding was first reported together with σ_1(Xe–CO),[25] these two virials provided the first instance of a temperature dependence of σ_1(Xe–A) which is in the opposite sign compared to all others observed for Xe with various collision partners. All other systems had the magnitude of the density coefficient of ^{129}Xe chemical shift decreasing with increasing temperature. Without a knowledge of the form of the intermolecular shielding function, an explanation for the unusual behavior of Xe in N_2 and Xe in CO could not be brought forward. We find here that the temperature dependence of σ_1(Xe–N_2) is a very sensitive test of the potential; we find that potentials constructed from the same set of dispersion coefficients (TNTB and ours) but with different repulsive parts do not give the same sign of the temperature dependence.

The shapes of the various surfaces at the global minimum are clearly different from each other. The quantum diffusion Monte Carlo solutions for the vibrational ground state using these various potential functions provide the average geometry, the average rotational constants and the dissocia-

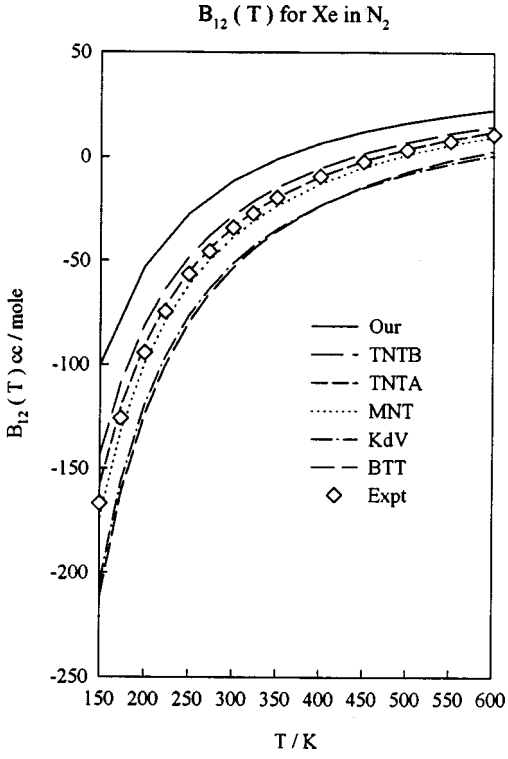

FIG. 8. The pressure second virial coefficient predicted by various potential surfaces and our Xe–N_2 PES are compared against the experimental data. The experimental points at 173, 223, 273, and 323 K are from the measurements of Brewer and the other experimental points are based on Brewer's universal correlating equation for second virial coefficients using a corresponding states approach (Ref. 62).

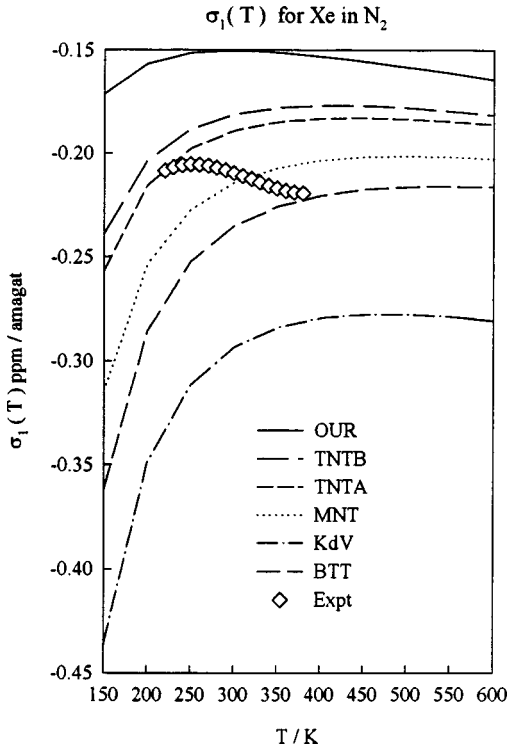

FIG. 9. The predicted second virial coefficients of ^{129}Xe nuclear shielding for Xe–N_2 calculated by averaging the *ab initio* Xe–N_2 intermolecular shielding surface using various potentials are compared with the experimental data obtained in the gas phase (Ref. 24).

tion energy of the complex from its ground vibrational state. The results are shown in Table VI. We do not have experimental spectroscopic data to compare with, however.

The Xe–CO system

The intermolecular shielding values and the fitted function of the form given in Eq. (2) for ^{129}Xe in Xe–CO are shown in Fig. 10. This angle-dependent description gives a reasonably good description of the calculated values. The root-mean-square deviation of this fit was 2.58 ppm. This is a highly anisotropic shielding surface, with the C end of the CO molecule (θ=180°) providing a greater magnitude of deshielding at equal distances from the center of mass. Part, but not all of this anisotropy has to do with the center of mass being closer to the O end of the molecule. If we compare the values at equal distances of Xe from the C and O nuclei, we find that in the collinear arrangement, the intermolecular Xe shielding is −24.67 ppm at R(Xe–O) = 3.4 Å, whereas it is −106.24 ppm at R(Xe–C) = 3.4 Å, and they are respectively −5.08 and −25.87 ppm at R(Xe–O) and R(Xe–C) = 4.0 Å. We note that Eq. (2) does not have the correct derivatives with respect to θ in the range θ=0°–40° to reproduce the detailed shape of the shielding surface in this range of angles at short distances. Nevertheless, the overall fit is reasonably good. A description based on a sum of site–site functions, Xe–O, and Xe–C, as in Eq. (2) gives a poorer fit, with a root-mean-square deviation of

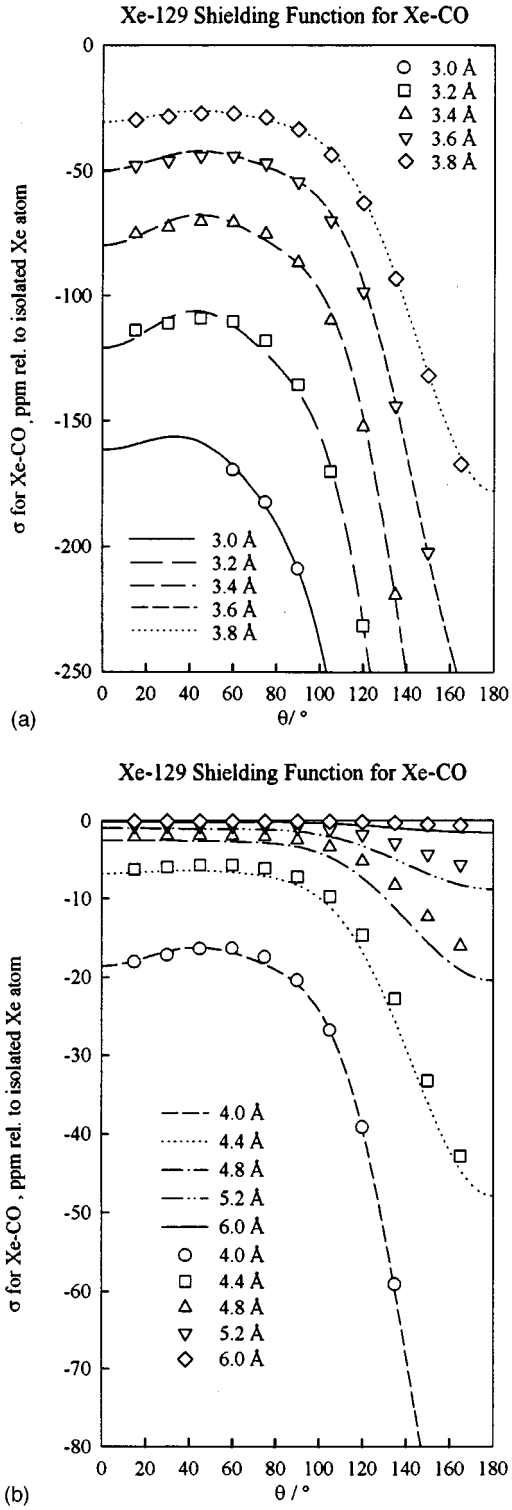

FIG. 10. The ^{129}Xe intermolecular shielding surface from *ab initio* calculations in Xe–CO and the fitted function of the form given in Eq. (2).

nearly 10 ppm. The shape of the intermolecular shielding function is complementary to that of the short-range part of the potential shown in Fig. 11.

The characteristics of the potential function for the Xe–CO system constructed in this work, using damped dispersion terms according to Eq. (10)–(12), and dispersion co-

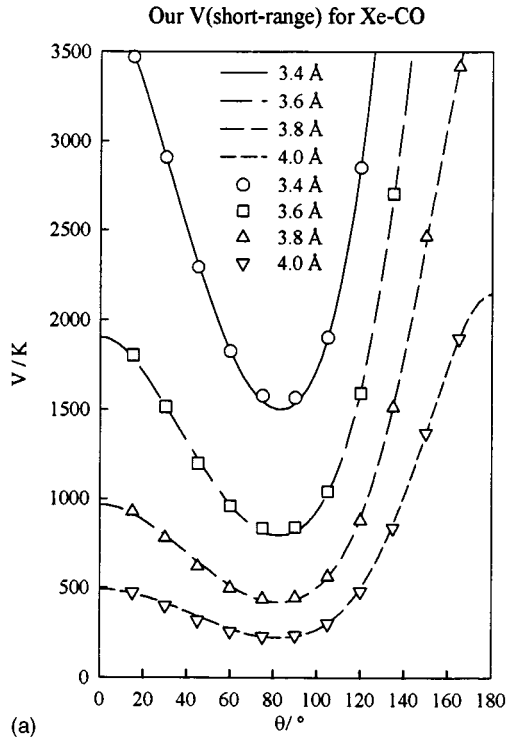

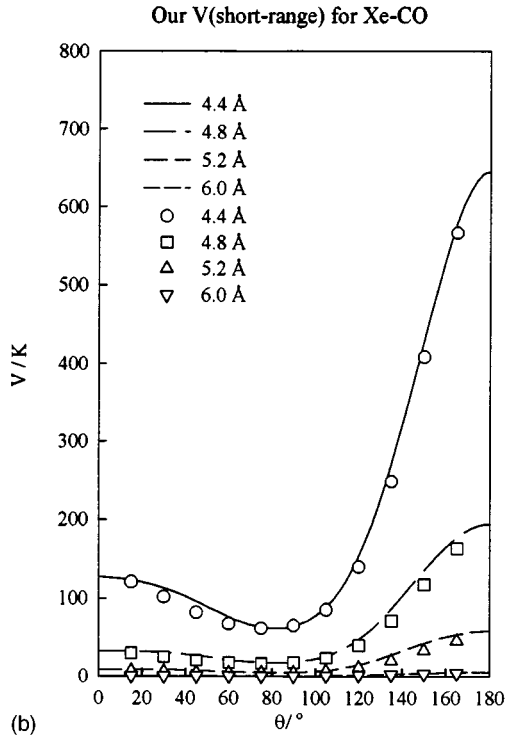

FIG. 11. *Ab initio* values for V^{short} for Xe–CO and the fitted functions of the form given in Eq. (6)–(8), to be compared with Fig. 10.

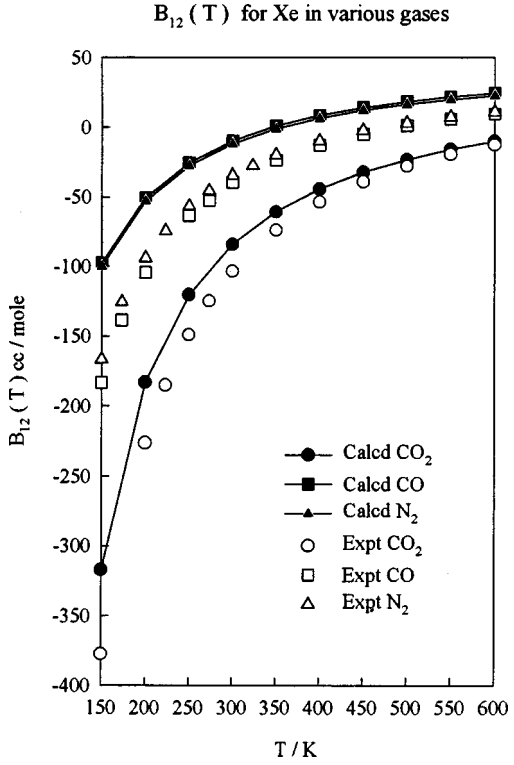

FIG. 12. The pressure second virial coefficient predicted by the potential-energy surfaces which have been constructed in this work are compared with the experimental data. The experimental points at 173, 223, 273, and 323 K are from Brewer and the other experimental points are based on Brewer's universal correlating equation for second virial coefficients using a corresponding states approach (Ref. 62).

efficients from Hettema *et al.*[37] are shown in Table IV compared with our PES for Xe–CO_2 and Xe–N_2. The global minimum in the potential-energy surface is at 4.183 Å and θ=88.7°; the rotational barrier at the oxygen end is low (5.2 cm^{-1}) while the rotational barrier at the carbon end is high (55.5 cm^{-1}). The difference between the rotational barriers for the rare gas atom at the two ends of the CO molecule is greater for Xe–CO than had been found for Ar–CO.[78]

Our potential function for Xe–CO only finds 52% and 33% of the experimental pressure second virial coefficient values at 173 and 273 K.[62] The results are shown in Fig. 12 together with the other potential-energy surfaces constructed in this work. Overall, the PES constructed in this work uniformly underestimate $B_{12}(T)$.

Using our calculated intermolecular shielding function for Xe–CO to calculate the second virial coefficient of the ^{129}Xe intermolecular nuclear shielding σ_1(Xe–CO) as in Eq. (16), we find the prediction of our Xe–CO potential function for the temperature dependence of this observable. As we can see in Fig. 13, our potential gives a reasonable agreement with the experimental temperature dependence of the density coefficients of ^{129}Xe chemical shifts that we had measured in mixtures of Xe and CO as well as Xe in N_2.[25] Our potential provides the right behavior with temperature, recovering 62% of the experimental value at 300 K. The unusual behaviors of σ_1(Xe–N_2) and σ_1(Xe–CO) in contrast to the temperature dependence of σ_1(Xe–CO_2) and σ_1(Xe–Xe) are both accounted for.

Spectroscopic constants predicted from this potential are shown in Table VII. The only available spectroscopic data on the Xe–CO van der Waals complex is from Johns *et al.*[79] They found that the rotational constant $B=0.0415\ cm^{-1}$, B

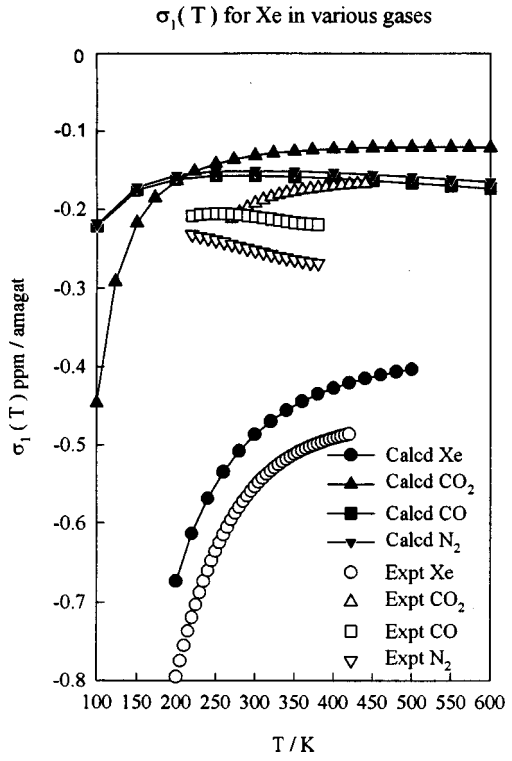

FIG. 13. The predicted second virial coefficients of ^{129}Xe nuclear shielding for mixtures of Xe–CO_2, Xe–N_2, and Xe–CO calculated by averaging the *ab initio* shielding surfaces over the potential-energy surfaces which have been constructed in this work are compared with the experimental data obtained in the gas phase (Refs. 24 and 25) and with the second virial coefficient for Xe–Xe (Refs. 23 and 91).

$-C=0.0015\ \mathrm{cm}^{-1}$, $D=0.40\times10^{-6}\ \mathrm{cm}^{-1}$, and $\Delta\nu$ (the shift in the origin of the complex band relative to the CO monomer)$=-0.867\ \mathrm{cm}^{-1}$. They deduced nearly a 90° angle and the ''effective intermolecular separations'' of 4.195 Å. We find that we have a larger average value of R(4.359 Å) and an average angle $\langle\theta\rangle$ close to 70°, and these translate to smaller rotational constants than experiment.

TABLE VII. Predictions of spectroscopic constants for Xe–CO from our potential.

Observable	Expt.	Prediction
k_s, mdyne/Å		0.008 182[a]
k_b, mdyne·Å		0.001 931[a]
$\langle C^2\rangle/\rho$ cm^{-2}/amagat		350[b]
$\langle R_m\rangle$, Å	4.195[d]	4.3595(9)[c]
$\langle\theta\rangle$, °	~90[d]	71.27(13)[c]
A, MHz		$279(54)\times10^{3}$[c]
B, MHz	1244[d]	1154.73(49)[c]
C, MHz	1200[d]	1136.49(48)[c]
D_0, cm^{-1}		76.56(7)[c]

[a]From analytic derivatives of the potential function at the global minimum.
[b]From integration according to Eq. (18).
[c]From quantum diffusion Monte Carlo solution of the van der Waals vibrational motion. These are averages over the ground-state vibrational wave functions.
[d]From Ref. 79, $B=0.0415\ \mathrm{cm}^{-1}$ and $(B-C)=0.0015\ \mathrm{cm}^{-1}$.

DISCUSSION

We have calculated the ^{129}Xe intermolecular shielding surfaces in the interaction of Xe with a linear molecule and have found that these surfaces are highly anisotropic. The intermolecular shielding surfaces seem to have a complementary behavior with respect to the repulsive part of the potential: Where the latter is large positive, the intermolecular shielding surface is large negative. This becomes most obvious in the unsymmetrical case, Xe–CO, comparing Fig. 10 with Fig. 11. The extent to which the shielding surface is expressed in the observed density coefficient of the nuclear shielding of course depends on the weighting of various parts of the surface by the Boltzmann factor which has the entire potential in it, repulsive plus dispersion. This means that the large deshielding which accompanies the geometries with the large repulsive energies will contribute to the observed density coefficient only to the extent that is permitted by the dispersion part of the potential energy. When the dispersion part is large enough to compensate for the large repulsive energies to give a reasonable Boltzmann factor, the large negative deshielding accompanying these large repulsive terms will be weighted favorably. This therefore is the complementary way in which dispersion plays a key role in the magnitudes of intermolecular shifts. In the early interpretations of the solvent effects on the Xe NMR chemical shift it had been assumed that dispersion played an important role, and that this could be expressed in terms of the shielding response to the mean-square fluctuating electric field that is implicit in the London model for dispersion forces.[80] Later on, it was shown that the coefficient for such a quadratic response to electric fields for Xe atom was orders of magnitude too small to account for the observed intermolecular chemical shifts.[81] The original intuitive ideas that dispersion plays an important role in the Xe chemical shifts may now be associated with the complementary role played by dispersion contributions to the potential energy as described above. The dispersion contributions *to the intermolecular shielding surface itself* has not been calculated here, since these *ab initio* calculations are only at the coupled Hartree–Fock level. In the Ar–Ar system, it had been found that the dispersion contributions to the intermolecular shielding which can be calculated at the level of second order correlation are negligible at all distances.[16] We expect this to be the case also for Xe shielding in Xe atom interacting with CO_2 or even Xe.

We find that the pairwise sum of atom–atom contributions is inadequate to describe fully the intermolecular shielding surface at short distances where the anisotropy is very pronounced, as in these Xe-linear molecule cases. On the other hand, the intermolecular shielding of a Xe atom interacting with two CO_2 molecules could probably be well described by a sum of two functions, each one in a form given by Eq. (1). Thus, summing over Xe-solvent molecule shielding functions for various configurations of Xe surrounded by the first solvation shell in a liquid may give acceptable results. Where the solvent molecule is much more complex, such as for a Xe atom in the presence of a zeolite cage, the description of the intermolecular shielding surface

becomes very problematical. In such cases, use of an intermolecular shielding function containing sums of atom–atom contributions appears to be the only practical choice, provided that shielding values for enough rare gas-zeolite fragment configurations are included in the fitting.[19]

We have calculated the entire ^{129}Xe shielding tensor at each of the 70, 70, and 130 geometries of Xe–CO_2, Xe–N_2, and Xe–CO, respectively. In this paper, we have only expressed the isotropic shielding in the form of a multidimensional surface. We have not considered how to best describe the elements of the tensor in a multidimensional surface, since not only do the three principal components of the tensor but also the orientation of the principal axes change with geometry. At $\theta=0°$ (and 180° in the case of Xe–CO) the nuclear site symmetry is high and the orientation of the principal axes of the tensor does not change with increasing distance. At $\theta=90°$ the site symmetry is C_{2v} for Xe–CO_2 and Xe–N_2 and there are three unique tensor components.[82] The axis directions remain unchanged with increasing distance: One is along the intermolecular vector, one is perpendicular to the plane of the supermolecule, and the third is in the plane of the molecule, perpendicular to the intermolecular vector. However, for $\theta=90°$ in the Xe–CO system or the general case of arbitrary θ values in any Xe-rigid linear molecule system, the nuclear site symmetry is C_s, the number of unique nonvanishing tensor components is five[82] and the relative magnitudes of the diagonal components are no longer simply related. The directions of the principal axis system also changes with geometry in this case. There are undoubtedly some very interesting insights which we have yet to discover. This will be considered in future work. For this time, we show only the change in the intermolecular shielding anisotropy ($\sigma_\parallel-\sigma_\perp$) for the $\theta=0°$ (and 180° in the case of Xe–CO) as a function of distance in Fig. 14. We note that the anisotropy drops off very sharply with distance, even faster than the isotropic shielding does. The isotropic shielding for the collinear configuration is $(\sigma_\parallel+2\sigma_\perp)/3$. The component parallel to the internuclear axis ($\sigma_\parallel$) is purely diamagnetic and does not change very fast, but the change in the component perpendicular to the internuclear axis with increasing distance is more pronounced since it has both diamagnetic and paramagnetic terms, and the paramagnetic term changes more drastically. Thus, the anisotropy ($\sigma_\parallel-\sigma_\perp$) has a more pronounced drop with increasing distance.

We have constructed what appear to be reasonable potential functions for Xe–CO_2, Xe–N_2, and Xe–CO in a straightforward way, without adjusting or scaling. We do find that they all underestimate the pressure second virial coefficient, recovering from 81% of the experimental value in Xe–CO_2 to about 50% in Xe–N_2, and about 40% in Xe–CO. In this way we know that the potential surfaces we have constructed here need improvement. Nevertheless, we find that when compared with other existing potential surfaces, only the Buck potential for Xe–CO_2 does better than ours. For Xe–N_2, none of the existing PES do as well as ours in accounting for the second virial coefficient of shielding. Our potential-energy surfaces provide the correct behavior of the second virial coefficient of nuclear shielding with increasing

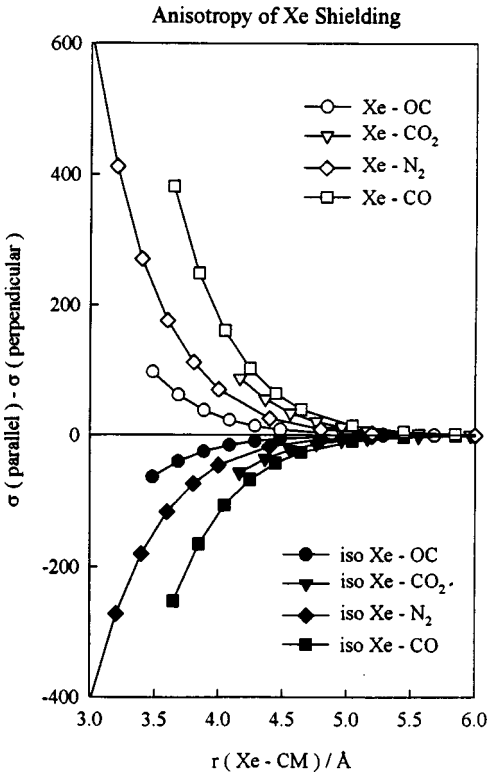

FIG. 14. The anisotropy of the ^{129}Xe shielding tensor for the collinear configurations of Xe–CO_2, Xe–N_2, Xe–CO, and Xe–OC varies with distance. Except for the sign, the behavior is analogous to the variation of the ^{129}Xe isotropic shielding in the collinear configuration (also shown here, relative to the free atom).

temperature. The change in the temperature behavior in going from Xe–CO and Xe–N_2 to Xe–CO_2 and Xe–Xe is well reproduced, as can be seen in Fig. 13. We find here that the temperature dependence of σ_1 is a very sensitive test of the potential although the magnitude of the density coefficient at room temperature does correlate with the isotropic average well depth.

It is disappointing that the constructed functions did not predict observables as well as we had hoped. We have found that even in the case of CO_2–Ar where the *ab initio* calculations were carried out at MP4 level using large basis sets,[83] the constructed PES did not perform in a uniformly superior manner to other more approximate potentials.[84] The next step would be to fix up the PES functions constructed here by some method of scaling so as to at least give good agreement with pressure second virial coefficients, without doing too much damage to the temperature dependence of the second virial coefficient of the Xe shielding. Once the functions have been improved, testing against other observables can proceed. For N_2–Xe there are two experimental relaxation cross sections that are extremely sensitive to the anisotropy of the potential.[85,86] These can be calculated by classical trajectory methods for any given PES, as we have already done for CO_2–Ar, N_2–Kr_1, and N_2–Xe.[69,76,77,84] The magnitude and the temperature dependence of these two independent cross sections serve as critical tests of any PES. In addition, there are some thermophysical properties which such classi-

cal trajectory results can be compared with, such as diffusion coefficients for Xe–N_2 and Xe–CO_2,[87,88] and mixture viscosities for Xe–CO_2.[89] Furthermore, there are collision-induced rotational perturbations which have been measured for Xe–CO_2 by Bulanin *et al.* at 291 K;[65] the first and zeroth spectral moments α_1 and γ_1 for the intensity due to induction in pairs of dissimilar molecules have been reported by Andreeva *et al.* at 295 K.[90] For a quantitative interpretation, these however require not only the anisotropic intermolecular potential surface but also a dipole moment surface.

CONCLUSIONS

We have calculated the ^{129}Xe intermolecular shielding surfaces in the interaction of Xe with a linear molecule using a fairly large basis set for the Xe atom. We have found that these surfaces are highly anisotropic. An important finding in this work is that the anisotropy of the intermolecular shielding surfaces can be described very well by using the same types of expansions in the $P_n(\cos\theta)$ as have been found to be satisfactory for describing the anisotropy of potential-energy surfaces. To the best of our knowledge, this is the first determination of the anisotropy of the full intermolecular shielding surface. The angular dependence of the surface has been examined in detail. The intermolecular shielding surfaces seem to have a complementary behavior with respect to the repulsive part of the potential: Where the latter is large positive, the intermolecular shielding surface is large negative. This becomes most obvious in the unsymmetrical case, Xe–CO. These intermolecular shielding surfaces determine the observed solvent effects on NMR chemical shifts of Xe. The most quantitative comparisons are made with the gas-phase density coefficients of the Xe chemical shifts that have been measured in the mixture of Xe with other gases.

The potential surfaces we have constructed here need improvement. It is customary to scale the dispersion and the induction terms by a factor greater than 1.0, leading to deeper potential wells, to account for the deficiencies associated with the use of a limited multipole expansion. We have not done any scaling of the dispersion and induction terms. Nevertheless, our potential-energy surfaces do provide the correct behavior of the second virial coefficient of ^{129}Xe nuclear shielding with increasing temperature. The change in the temperature behavior in going from Xe–CO and Xe–N_2 to Xe–CO_2 and Xe–Xe is well reproduced.

ACKNOWLEDGMENTS

This research was supported by the National Science Foundation (Grant CHE95-28066). A.C.D. acknowledges support from the Camille and Henry Dreyfus Foundation. The authors are grateful to Emily M. Earle for assistance in the shielding calculations.

[1] J. A. Ripmeester, C. I. Ratcliffe, and J. S. Tse, J. Chem. Soc., Faraday Trans. 1 **84**, 3731 (1988).
[2] F. Lee, E. Gabe, J. S. Tse, and J. A. Ripmeester, J. Am. Chem. Soc. **110**, 6014 (1988).
[3] J. Fraissard and T. Ito, Zeolites **8**, 350 (1988).
[4] C. Dybowski, N. Bansal, and T. M. Duncan, Ann. Rev. Phys. Chem. **42**, 433 (1991).
[5] P. J. Barrie and J. Klinowski, Prog. NMR Spectrosc. **24**, 91 (1992).
[6] T. R. Stengle and K. L. Williamson, Macromolecules **20**, 1428 (1987).
[7] J. B. Miller, J. H. Walton, and C. M. Roland, Macromolecules **26**, 5602 (1993).
[8] A. P. M. Kentgens, H. A. van Boxtel, R. J. Verweel, and W. S. Veeman, Macromolecules **24**, 3712 (1991).
[9] S. B. Liu, B. M. Fung, T. C. Yang, E. C. Hong, C. T. Chang, P. C. Shih, F. H. Tong, and T. L. Chen, J. Phys. Chem. **98**, 4393 (1994).
[10] J. G. Kim, T. Kompany, R. Ryoo, T. Ito, and J. Fraissard, Zeolites **14**, 427 (1994).
[11] L. C. de Menorval, J. Fraissard, and T. Ito, J. Chem. Soc., Faraday Trans. 1 **78**, 403 (1982).
[12] *Zeolites and Related Microporous Materials: State of the Art 1994*, edited by J. Weitkamp, H. G. Karge, H. Pfeifer, and W. Hölderich (Elsevier, Amsterdam, 1994), pp. 757, 765, 749.
[13] L. Maistriau, E. G. Derouane, and T. Ito, Zeolites **10**, 311 (1990).
[14] C. J. Jameson, A. K. Jameson, and S. M. Cohen, J. Chem. Phys. **62**, 4224 (1975).
[15] C. J. Jameson, A. K. Jameson, and S. M. Cohen, J. Chem. Phys. **65**, 3401, 5226 (1976).
[16] C. J. Jameson and A. C. de Dios, J. Chem. Phys. **97**, 417 (1992).
[17] C. J. Jameson and A. C. de Dios, J. Chem. Phys. **98**, 2208 (1993).
[18] C. J. Jameson and A. C. de Dios, in *Nuclear Magnetic Shielding and Molecular Structure*, edited by J. A. Tossell (Kluwer Academic, Dordrecht, 1993), pp. 95–116.
[19] C. J. Jameson and H. M. Lim, J. Chem. Phys. **103**, 3885 (1995).
[20] W. Kutzelnigg, C. van Wullen, U. Fleischer, R. Franke, and T. van Mourik, in *Nuclear Magnetic Shielding and Molecular Structure*, edited by J. A. Tossell (Kluwer Academic, Dordrecht, 1993), pp. 141–161.
[21] C. J. Jameson and H. S. Gutowsky, J. Chem. Phys. **40**, 1714 (1964).
[22] C. J. Jameson and J. Mason, in *Multinuclear Nuclear Magnetic Resonance*, edited by J. Mason (Plenum, London, 1987), Chap. 3.
[23] A. C. de Dios and C. J. Jameson (unpublished).
[24] C. J. Jameson, A. K. Jameson, and S. M. Cohen, J. Chem. Phys. **66**, 5226 (1977).
[25] C. J. Jameson, A. K. Jameson, and H. Parker, J. Chem. Phys. **68**, 3943 (1978).
[26] K. Wolinski, J. Hinton, and P. Pulay, J. Am. Chem. Soc. **112**, 8251 (1990).
[27] M. Schindler and W. Kutzelnigg, J. Chem. Phys. **76**, 1919 (1982).
[28] W. Kutzelnigg, M. Schindler, and U. Fleischer, in *NMR Basic Principles and Progress* (Springer, Berlin, 1990), Vol. 23.
[29] A. E. Hansen and T. D. Bouman, J. Chem. Phys. **82**, 5035 (1985).
[30] J. C. Facelli, D. M. Grant, T. D. Bouman, and A. E. Hansen, J. Comp. Chem. **11**, 32 (1990).
[31] T. A. Keith and R. F. W. Bader, Chem. Phys. Lett. **191**, 614 (1992).
[32] V. G. Malkin, O. L. Malkina, L. A. Eriksson, and D. R. Salahub, in *Modern Density Functional Theory: A Tool for Chemistry*, Vol. 2 of *Theoretical and Computational Chemistry*, edited by P. Politzer and J. M. Seminario (Elsevier, Amsterdam, 1995), p. 273; G. Schreckenbach, R. M. Dickson, Y. Ruiz-Morales, and T. Ziegler, in *Density Functional Theory in Chemistry*, edited by B. Laird, R. Ross, and T. Ziegler (American Chemical Society, Washington, D. C., 1996).
[33] H. Partridge and K, Faegri, NASA Technical Memo 103918 (1992).
[34] D. A. Bishop and S. M. Cybulski, Chem. Phys. Lett. **211**, 255 (1993).
[35] S. Huzinaga, *Gaussian Basis Sets for Molecular Calculations* (Elsevier, Amsterdam, 1984).
[36] A. D. Buckingham, P. W. Fowler, and J. M. Hutson, Chem. Rev. **88**, 963 (1988); M. J. Frisch, G. W. Trucks, H. B. Schlegel, P. M. W. Gill, B. G. Johnson, M. A. Robb, J. R. Cheeseman, T. Keith, G. A. Petersson, J. A. Montgomery, K. Raghavachari, M. A. Al-Laham, V. G. Zakrzewski, J. V. Ortiz, J. B. Foresman, J. Cioslowski, B. B. Stefanov, A. Nanayakkara, M. Challacombe, C. Y. Peng, P. Y. Ayala, W. Chen, M. W. Wong, J. L. Andres, E. S. Replogle, R. Gomperts, R. L. Martin, D. J. Fox, J. S. Binkley, D. J. Defrees, J. Baker, J. P. Stewart, M. Head-Gordon, C. Gonzalez, and J. A. Pople, GAUSSIAN 94, Revision C.2, Gaussian, Inc., Pittsburgh, PA, 1995.
[37] H. Hettema, P. E. S. Wormer, and A. J. Thakkar, Mol. Phys. **80**, 533 (1993).
[38] R. T Pack, J. Chem. Phys. **74**, 1659 (1976).
[39] K. T. Tang and J. P. Toennies, J. Chem. Phys. **80**, 3726 (1984).

[40] J. H. vanLenthe, J. G. C. M. van Duijneveldt-van de Rijdt, and F. B. van Duijneveldt, Adv. Chem. Phys. **69**, 521 (1987).
[41] G. Chalasinski and M. Gutowski, Chem. Rev. **88**, 943 (1988).
[42] S. F. Boys and F. Bernardi, Mol. Phys. **19**, 538 (1970).
[43] J. B. Anderson, J. Chem. Phys. **63**, 1499 (1975).
[44] J. B. Anderson, J. Chem. Phys. **65**, 4121 (1976).
[45] V. Buch, J. Chem. Phys. **97**, 726 (1992).
[46] P. Sandler, J. O. Jung, M. M. Szczesniak, and V. Buch, J. Chem. Phys. **101**, 1378 (1994).
[47] K. A. Franken and C. E. Dykstra, Chem. Phys. Lett. **220**, 161 (1994).
[48] M. H. Kalos, Phys. Rev. A **2**, 250 (1970).
[49] B. J. Adler and D. M. Ceperley, J. Chem. Phys. **81**, 5833 (1984).
[50] M. A. Suhm and R. O. Watts, Phys. Rep. **204**, 293 (1991).
[51] M. Iida, Y. Ohshima, and Y. Endo, J. Phys. Chem. **97**, 357 (1993).
[52] E. B. Wilson J. C. Decius, and P. C. Cross, *Molecular Vibrations* (Dover, New York, 1980).
[53] S. Li and E. R. Bernstein, J. Chem. Phys. **95**, 1577 (1991).
[54] R. T Pack, J. Chem. Phys. **78**, 7217 (1983).
[55] R. T Pack, Chem. Phys. Lett. **55**, 197 (1978).
[56] C. Dreyfus, L. Berreby, and E. Dayan, Chem. Phys. Lett. **79**, 476 (1981).
[57] R. L. Armstrong, J. M. Blumenfeld, and C. G. Gray, Can. J. Phys. **46**, 1331 (1968).
[58] U. Buck, F. Huisken, D. Otten, and R. Schinke, Chem. Phys. Lett. **101**, 126 (1983).
[59] G. Billing, Chem. Phys. Lett. **117**, 145 (1985).
[60] C. Dreyfus, private communications to G. Billing (Ref. 59).
[61] R. T Pack, J. Chem. Phys. **61**, 2109 (1974).
[62] J. Brewer, Determination of Mixed Virial Coefficients, Tech. Rept. AADD 663448, AFOSR No. 67-2795, Air Force Office of Scientific Research, Arlington VA, 1967.
[63] L. Berreby and E. Dayan, Mol. Phys. **48**, 581 (1983).
[64] L. Berreby and E. Dayan, Chem. Phys. Lett. **243**, 85 (1995).
[65] M. O. Bulanin, M. V. Tonkov, and N. N. Filippov, Can. J. Phys. **62**, 1306 (1984).
[66] R. W. Randall, M. A. Walsh, and B. J. Howard, Faraday Discuss. Chem. Soc. **85**, 13 (1988).
[67] U. Buck, D. Otten, R. Schinke, and D. Poppe, J. Chem. Phys. **82**, 202 (1985).
[68] P. G. Kistemaker and A. E. de Vries, Chem. Phys. **7**, 371 (1975).
[69] Marc ter Horst, Ph. D. thesis, University of Illinois at Chicago, 1993.
[70] M. S. Bowers, K. T. Tang, and J. P. Toennies, J. Chem. Phys. **88**, 5465 (1988).
[71] C. Nyeland and J. P. Toennies, Chem. Phys. **122**, 337 (1988).
[72] A. J. Thakkar, H. Hettema, and P. E. S. Wormer, J. Chem. Phys. **97**, 3252 (1992).
[73] F. R. W. McCourt (private communications).
[74] F. Visser, P. E. S. Wormer, and P. Stam, J. Chem. Phys. **79**, 4973 (1983).
[75] L. Beneventi, P. Casavecchia, G. G. Golpi, C. C. K. Wong, and F. R. W. McCourt, J. Chem. Phys. **98**, 7926 (1993).
[76] M. A. ter Horst and C. J. Jameson, J. Chem. Phys. **102**, 4431 (1995).
[77] F. R. W. McCourt, M. A. ter Horst, and C. J. Jameson, J. Chem. Phys. **102**, 5752 (1995).
[78] V. Castells, N. Halberstadt, S. K. Shin, R. A. Beuaudet, and C. Wittig, J. Chem. Phys. **101**, 1006 (1994).
[79] J. W. C. Johns, Z. Lu, and A. R. W. McKellar, J. Mol. Spectrosc. **159**, 210 (1993).
[80] W. T. Raynes, A. D. Buckingham, and H. J. Bernstein, J. Chem. Phys. **36**, 3481 (1962).
[81] D. M. Bishop and C. M. Cybulski, Chem. Phys. Lett. **211**, 255 (1993).
[82] A. D. Buckingham and S. M. Malm, Mol. Phys. **22**, 1127 (1971).
[83] P. J. Marshall, M. M. Szczesniak, J. Sadlej, G. Chalasinski, M. A. ter Horst, and C. J. Jameson, J. Chem. Phys. **104**, 6569 (1996).
[84] M. A. ter Horst and C. J. Jameson, J. Chem. Phys. **104**, 6787 (1996).
[85] C. J. Jameson, A. K. Jameson, and N. C. Smith, J. Chem. Phys. **86**, 6833 (1987).
[86] C. J. Jameson, A. K. Jameson, and M. A. ter Horst, J. Chem. Phys. **95**, 5799 (1991).
[87] A. S. M. Wahby, Physica C **145**, 78 (1987).
[88] H. L. Robjohns and P. J. Dunlop, Ber. Bunsenges. Phys. Chem. **85**, 655 (1981).
[89] J. Kestin and S. T. Ro, Ber. Bunsenges. Phys. Chem. **74**, 619 (1978).
[90] G. V. Andreeva, A. A. Kudryavtsev, M. V. Tonkov, and N. N. Filippov, Opt. Spectrosc. (USSR) **68**, 623 (1990).
[91] C. J. Jameson, A. K. Jameson, and S. M. Cohen, J. Chem. Phys. **59**, 4540 (1973).
[92] A. D. Buckingham, C. Graham, and J. H. Williams, Mol. Phys. **49**, 703 (1983).
[93] G. Birnbaum and E. R. Cohen, Mol. Phys. **32**, 161 (1976).
[94] J. S. Muenter, J. Mol. Spectrosc. **55**, 490 (1975).
[95] W. L. Meerts, F. H. de Leeuw, and A. Dymanus, Chem. Phys. **22**, 319 (1977).